QUANTUM PLASMAS

Professor coordinator:

Vanea Covlea

Students:

Group 401

Faculty of Physics
January25 2012

TABLE OF CONTENTS

I. Plasma. An Analysis

1. History

Plasma was first identified in a Crookes tube, and so described by Sir William Crookes in 1879 (he called it "radiant matter"). The nature of the Crookes tube "cathode ray" matter was subsequently identified by British physicist Sir J.J. Thomson in 1897.The term "plasma" was coined by Irving Langmuir in 1928, perhaps because the glowing discharge molds itself to the shape of the Crooks tube.

Except near the electrodes, where there are sheaths containing very few electrons, the ionized gas contains ions and electrons in about equal numbers so that the resultant space charge is very small. We shall use the name plasma to describe this region containing balanced charges of ions and electrons.

2. Definition of a plasma

Plasma is loosely described as an electrically neutral medium of positive and negative particles (i.e. the overall charge of a plasma is roughly zero). It is important to note that although they are unbound, these particles are not 'free'. When the charges move they generate electrical currents with magnetic fields, and as a result, they are affected by each other's fields. This governs their collective behavior with many degrees of freedom.A definition can have three criteria:

(1)*The plasma approximation*: Charged particles must be close enough together that each particle influences many nearby charged particles, rather than just interacting with the closest particle (these collective effects are a distinguishing feature of a plasma). The plasma approximation is valid when the number of charge carriers within the sphere of influence (called the Debye sphere whose radius is the Debye screening length) of a particular particle is higher than unity to provide collective behavior of the charged particles. The average number of particles in the Debye sphere is given by the plasma parameter, "Λ" (the Greek letter Lambda).

(2)*Bulk interactions*: The Debye screening length (defined above) is short compared to the physical size of the plasma. This criterion means that interactions in the bulk of the plasma are more important than those at its edges, where boundary effects may take place. When this criterion is satisfied, the plasma is quasineutral.

(3)*Plasma frequency*: The electron plasma frequency (measuring plasma oscillations of the electrons) is large compared to the electron-neutral collision frequency (measuring frequency of collisions between electrons and neutral particles). When this condition is valid, electrostatic interactions dominate over the processes of ordinary gas kinetics.

Ranges of plasma parameters

Plasma parameters can take on values varying by many orders of magnitude, but the properties of plasmas with apparently disparate parameters may be very similar (see plasma scaling). The following chart considers only conventional atomic plasmas and not exotic phenomena like quark gluon plasmas:

Typical ranges of plasma parameters: orders of magnitude (OOM)

Characteristic	Terrestrial plasmas	Cosmic plasmas
Size in meters	10^{-6} m (lab plasmas) to 10^2 m (lightning) (~8 OOM)	10^{-6} m (spacecraft sheath) to 10^{25} m (intergalactic nebula) (~31 OOM)
Lifetime in seconds	10^{-12} s (laser-produced plasma) to 10^7 s (fluorescent lights) (~19 OOM)	10^1 s (solar flares) to 10^{17} s (intergalactic plasma) (~16 OOM)
Density in particles per cubic meter	10^7 m^{-3} to 10^{32} m^{-3} (inertial confinement plasma)	1 m^{-3} (intergalactic medium) to 10^{30} m^{-3} (stellar core)
Temperature in kelvins	~0 K (crystalline non-neutral plasma[10]) to 10^8 K (magnetic fusion plasma)	10^2 K (aurora) to 10^7 K (solar core)
Magnetic fields in teslas	10^{-4} T (lab plasma) to 10^3 T (pulsed-power plasma)	10^{-12} T (intergalactic medium) to 10^{11} T (near neutron stars)
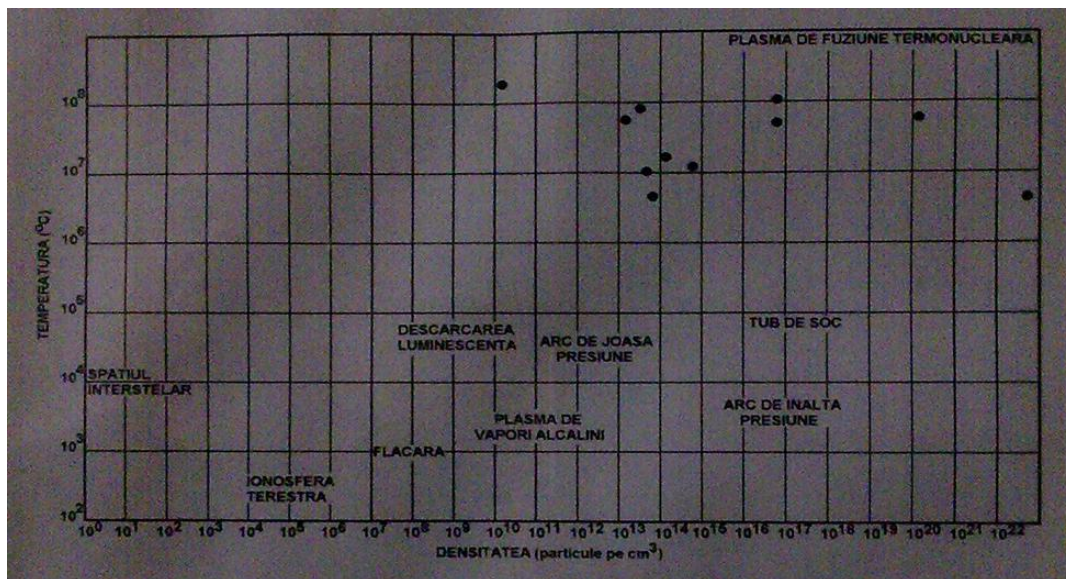
3. **Spark Discharge**

Spark discharge appears like a beam of thin shiny wires which are ramifying in a zig-zag way. They take place instantly in the discharge interval, they quickly disappear and they replace one with another. Spark discharge occurs when the gas pressure is high. In these conditions the ignition voltage is very high, but immediately, after the discharge interval is pierced by a spark channel, its resistance becomes very weak and in the circuit appears a strong current leading to a redistribution of the potential, therefore on the discharge interval remain a small potential difference.

When the gas between the electrodes finds an obstacle in the shape of a solid wall, spark discharge doesn't find a way to bypass the obstacle.

Ignition voltage of spark discharge

At an atmospheric pressure, when the configuration of the discharge interval doesn't allow the appearance of a corona discharge or when the current source power is not enough for the appearance and for the maintenance of a stationary arc discharge, spark discharge is the final stadium of the discharge progress.

Streamer theory

The discharge interval is pierced only by a single avalanche which causes the occurrence of a streamer which is quickly spread by the discharge interval.

4. Lightning

On clear days and nights there is a slow, steady, nearly uniform flow of electricity from the surface of the negatively charged earth and oceans to about 50 km up into the positively charged atmosphere. The net charge over the whole earth is about 10^6 C; the potential difference between the earth and the electrosphere is about 3.0E5 Volts; and the current density is about 1.0E-11 amps/m^2. Where there are no clouds, between the earth and the 50 kilometer elevation, the electric field may reach values as high as 100 volts per meter. In thunderclouds the electric field may be much higher. Lightning is the means by which electrons are transported back to the earth to "recharge" the earth to its negative polarity.

Solar energy is the ultimate source for creating lightning. Warmth from the sun's radiant energy is responsible for convection of air, snow, rain, and hail within clouds. Through frictional effects (very much like those which make static electricity when we walk across carpets) the flow of air masses and precipitating droplets cause separation of charges. Free charges created in the upper atmosphere by cosmic rays also play a role in the detailed behavior of lightning.

The electrical structure in thunderheads (generally cumulonimbus clouds) is complex. There are major differences between summer and winter thunderheads, and between those over Florida, New Mexico, South America and Japan. For the most common type of lightning, negative cloud to ground, there is a strong negative region in the lower section of the cloud. The base and top of the cloud may also have scattered positive regions.

The lightning flash is composed of several strokes. The first, called the stepped leader, originates from the cloud. It comprises brief (~ 1 ms) spikes in electrical current (to more than 1000 A) separated by times of lesser current (50 ms, ~100 A). This part of the lightning flash sets the jagged shape that the later, more intense return strokes (currents originating from the earth) will

follow. The return strokes may have currents in excess of 30 kA, each lasting for about 50 ms. A typical lightning flash transfers about 10 C from the atmosphere to the earth.

Ball-Lightning

Lightning-balls are less shiny and they have a slow spread through the atmosphere. Their duration is between fractions of seconds and several minutes.

Ionization of the atmosphere. Electric fields and atmospheric currents.

In all atmospheric layers, ionization occurs because of the components of cosmic radiation. A study regarding ionization of the inferior atmospheric layers is done by using the usual methods, for example, concentration determination and ion mobility and also determination of the potential distribution.

Lightning - Characteristic of a storm

As the ice particles within a cloud (called hydrometeors) grow and interact, they collide, fracture and break apart. It is thought that the smaller particles tend to acquire positive charge, while the larger particles acquire more negative charge. These particles tend to separate under the influences of updrafts and gravity until the upper portion of the cloud acquires a net positive charge and the lower portion of the cloud becomes negatively charged. This separation of charge produces enormous electrical potential both within the cloud and between the cloud and ground. This can amount to millions of volts, and eventually the electrical resistance in the air breaks down and a flash begins. Lightning, then, is an electrical discharge between positive and negative regions of a thunderstorm.

A lightning flash is composed of a series of strokes with an average of about four. The length and duration of each lightning stroke vary, but typically average about 30 microseconds. (The average peak power per stroke is about 10^{12} watts.)

Lightning in mythology

Lightning, the thunderbolt from mythology, has long been feared as an atmospheric flash of supernatural origins: the great weapon of the gods. The Greeks both marveled and feared lightning as it was hurled by Zeus. For the Vikings, lightning was produced by Thor as his hammer struck an anvil while riding his chariot across the clouds. In the East, early statues of Buddha show him carrying a thunderbolt with arrows at each end. Indian tribes in North America believed that lightning was due to the flashing feathers of a mystical bird whose flapping wings produced the sound of thunder.

A little bit of history...

Benjamin Franklin performed the first systematic, scientific study of lightning during the second half of the 18th century. Prior to that time, electrical science had developed to the point where positive and negative charges could be separated. Electrical machines could, by rubbing together two different materials, store the charges in primitive capacitors called Leyden Jars from which sparks could be generated and observed.

While others had previously noted the similarity between laboratory sparks and lightning, Franklin was the first to design an experiment which conclusively proved the electrical nature of lightning. In his experiment, he theorized that clouds are electrically charged, from which it follows that lightning must also be electrical. The experiment involved Franklin standing on an electrical stand, holding an iron rod with one hand to obtain an electrical discharge between the other hand and the ground. If the clouds were electrically charged then sparks would jump between the iron rod and a grounded wire, in this case, held by an insulating wax candle.

This experiment was successfully performed by Thomas Francois D'Alibard of France in May 1752 when sparks were observed to jump from the iron rod during a thunderstorm. G. W. Richmann, a Swedish physicist working in Russia during July 1753, proved that thunderclouds contain electrical charge, and was killed when lightning struck him.

Before Franklin accomplished his original experiment, he thought of a better way to prove his hypothesis through the use of a kite. The kite took the place of the iron rod, since it could reach a greater elevation and could be flown anywhere. During a Pennsylvania thunderstorm in 1752 the most famous kite in history flew with sparks jumping from a key tied to the bottom of damp kite string to an insulating silk ribbon tied to the knuckles of Franklin's hand. Franklin's grounded body provided a conducting path for the electrical currents responding to the strong electric field buildup in the storm clouds.

In addition to showing that thunderstorms contain electricity, by measuring the sign of the charge delivered through the kite apparatus, Franklin was able to infer that while the clouds were overhead, the lower part of the thunderstorm was generally negatively charged.

Little significant progress was made in understanding the properties of lightning until the late 19th century when photography and spectroscopic tools became available for lightning research.

Lightning current measurements were made in Germany by Pockels (1897-1900) who analyzed the magnetic field induced by lightning currents to estimate the current values. Time-resolved photography was used by many experimenters during the late l9th century to identify individual lightning strokes that make up a lightning discharge to the ground.

Lightning research in modern times dates from the work of C.T.R. Wilson who was the first to use electric field measurements to estimate the structure of thunderstorm charges involved in lightning discharges. Wilson, who won the Nobel Prize for the invention of the Cloud Chamber, made major contributions to our present understanding of lightning.

Research continued at a steady pace until the late 1960's when lightning research became particularly active. This increased interest was motivated both by the danger of lightning to aerospace vehicles and solid state electronics used in computers and other devices as well as by the improved measurement and observational capabilities which were made possible by advancing technology.

Plasma - Lightning – parametric analysis

$n_0 = 10^{20}$

$T_e (K) = 10^6$

Debye length	Landau length	Plasma frequency	Plasma condition
$\lambda_D^e = \sqrt{\dfrac{\varepsilon_0 k T_e}{e^2 N_0}}$	$\lambda_L = \dfrac{e^2}{6\pi\varepsilon_0 k T_e}$	$v_P = \dfrac{1}{2\pi}\left(\dfrac{e^2 N_0}{\varepsilon_0 m_e}\right)^{1/2}$	$N_0 \ll 10^{11} T_e^{3}$
$12{,}36*10^{11}$	$4{,}63*10^{5}$	$2{,}85*10^{11}$	YES

5. Ionosfera

Ionosfera reprezinta o "patura" de electroni, ioni si molecule, care inconjoara Pamantul, care incepe de pe la aproximativ 50 km pana la 1000 km. Existenta sa se datoreaza in principal radiatiilor UV provenite de la soare. Aceasta ionizare depinde deci de activitatea soarelui ceea ce face sa avem alte grade de ionizare ziua sau noaptea, si alte grade de ionizare in diferite sezoane ale anului. Alt aspect important il reprezinta si pozitia geografica, deoarece avem alt flux de particule provenite de la soare la poli, si altul la ecuator.
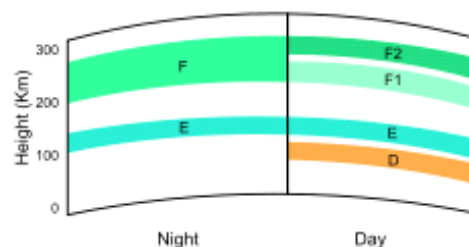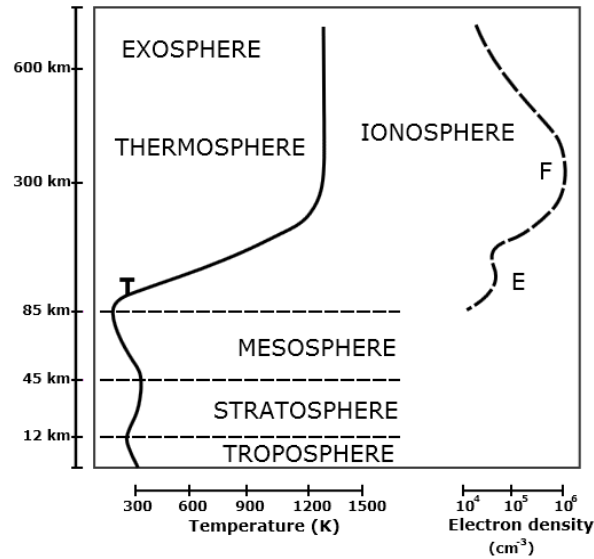
Stratul "D"

Este cea mai de jos subpatura a ionosferei, cuprinsa intre 60-90 km fata de suprafata Pamantului. Ionizarea in aceasta zona se datoreaza radiatiei alfa hidrogen din seria Lyman cu o lungime de unda de 121.5 nm ionizand oxidul de azot (NO). In plus, la o activitate a soarelui mare, razele X pot ioniza N_2 si O_2. Ca rezultat avem o frecventa mare a acestei zone, care nu reflecta undele radio, dar le atenueaza.

Stratul "E"

Stratul din mijlocul ionosferei, cuprins intre 90 – 120 km fata de suprafata Pamantului. Ionizarea aici se datoreaza razelor X slabe (1-10 nm), si razelor UV indepartate, care ionizeaza moleculele de O_2. La incidenta oblica, aceasta zona poate decat reflecta undele radio (< 10 MHz).

Stratul "F"

Se intinde de la aproximativ 200 km pana la mai bine de 500 km fata de suprafata Pamantului. Reprezinta zona cea mai densa a ionosferei. Dupa aceasta zona de afla asa numita "partea de sus" a ionosferei unde radiatiile UV extreme ionizeaza oxigenul atomic. Noaptea el formeaza un singur strat, dar pe timpul zilei apar distorsiuni, care poate incadra aceasta zona in doua parti distincte F_1 respectiv F_2.

Mecanismul de refractie al ionosferei

Cand o unda radio ajunge in ionosfera, campul electric al undei determina o oscilatie a electronilor din ionosfera cu o frecventa egala cu frecventa undei incidente. Aceasta oscilatie a electronilor poate fi pierduta prin procesul de recombinare, fie poate re-emite energia undei incidente. Refractie totala se poate produce daca frecventa ionosferei la "coliziune" este mai

mica decat frecventa undei radio, iar cand densitatea de electroni in ionosfera este suficient de mare.

Frecventa pe care trebuie sa o aibe o unda radio pentru a putea fi reflectata de o anumita zona a ionosferei, trebuie sa fie mai mica decat *frecventa critica :*

$$f_{critical} = 9 \times 10^{-3} \sqrt{N}$$

N = densitatea de electroni (cm^{-3})

$f_{critica}$ (MHz)

Formula de transformare a numarului de pete solare in flux:

$$F = 63.75 + 0.728 * S + 0.00089 * S^2$$

Formula de transformare a fluxului in numar de pete solare:

$$S = 33.52 * \sqrt{85.12 + F} - 408.99$$

6. Notiuni generale de Fizica Plasmei

La nivel microscopic, plasma se defineşte ca un ansamblu de particule neutre (atomi, molecule), particule încărcate cu sarcină electrică (electroni, ioni negativi, ioni pozitivi), cuante de radiaţie şi câmpuri electromagnetice aflate într-o continuă interacţiune. La nivel macroscopic, plasma poate fi definită ca un fluid conductor electric în care purtătorii de sarcină electrică se află într-un număr suficient de mare pentru a influenţa în mod decisiv proprietăţile mediului.

Câţiva parametri importanţi ce caracterizează plasma ar fi: lungimea *Debye*, sfera *Debye*, lungimea *Landau*, frecvenţa plasmei, frecvenţa *Larmor*, raza *Larmor*.

Se defineşte **lungimea Debye** λ_D^e **a electronilor din plasmă** (lungimea *Debye* de ecranare a ionilor de către electroni) din relaţia:

$$\lambda_D^e = \sqrt{\frac{\varepsilon_0 k T_e}{e^2 N_0}}$$

în care: T_e este temperatura electronilor, iar N_0 este densitatea purtătorilor de sarcină electrică din plasmă.

Potenţialul coulombian ecranat al ionului pozitiv test cu sarcină electrică +*e* are forma:

$$V(r) = \frac{e}{4\pi\varepsilon_0 r} \exp\left(-\frac{r}{\lambda_D^e}\right)$$

Se defineşte **lungimea _Debye_ λ_D^i a ionilor din plasmă** (lungimea _Debye_ de ecranare a electronilor de către ioni) din relaţia:

$$\lambda_D^i = \sqrt{\frac{\varepsilon_0 k T_i}{e^2 N_0}}$$

în care: T_i este temperatura ionilor.

Potenţialul coulombian ecranat al electronului test cu sarcină electrică _-e_ are forma:

$$V(r) = \frac{-e}{4\pi\varepsilon_0 r} \exp\left(-\frac{r}{\lambda_D^i}\right)$$

Putem interpreta lungimea _Debye_ ca fiind acea distanţă din plasmă la care, în condiţiile de ecranare a purtătorilor de sarcină electrică, potenţialul coulombian ecranat al particulei test libere scade de _e_ ori. O caracteristică esenţială a lungimii _Debye_ este aceea că ea defineşte dimensiunea minimă a volumului ocupat de plasmă. Volumul sferic cu raza egală cu lungimea _Debye_ poartă numele de _sferă Debye_. La analiza diferitelor fenomene din plasmă, trebuie să se facă deosebire între procesele care au loc în exteriorul sferei _Debye_, respectiv în interiorul sferei _Debye_.

Lungimea Landau λ_L este definită ca distanţa medie dintre purtătorii de sarcină la care energia cinetică a electronilor este egală cu energia lor potenţială. În cazul electronului aflat în câmpul coulombian al unui ion simplu ionizat, lungimea _Landau_ este dată de relaţia:

$$\lambda_L = \frac{e^2}{6\pi\varepsilon_0 k T_e}$$

O altă mărime caracteristică plasmei este **frecvenţa plasmei** ν_P. Abaterii spaţiale microscopice de la cvasineutralitatea plasmei, îi corespunde o abatere microscopică temporală. Această abatere este rezultatul tendinţei plasmei de a rămâne cvasineutră la nivel macroscopic. Micile fluctuaţii temporale ale plasmei de la starea de cvasineutralitate macroscopică, dau naştere la câmpuri electrice de aşa natură încât electronii vor fi antrenaţi într-o mişcare oscilatorie cu frecvenţa ν_P:

$$\nu_P = \frac{1}{2\pi} \left(\frac{e^2 N_0}{\varepsilon_0 m_e}\right)^{1/2}$$

Această relație a fost obținută făcând următoarele aproximații: ionii se află în stare de repaus, iar electronii sunt considerați reci. Aceștia iau viteze numai datorită apariției câmpurilor electrice rezultate în urma abaterilor microscopice de la cvasineutralitate. De asemenea, pe durata abaterii temporale de la cavsineutralitate, în plasmă nu iau naștere, respectiv nu dispar purtători de sarcină electrică. Așadar, frecvența plasmei a fost obținută într-un model idealizat. Luarea în considerare a temperaturii plasmei va duce la o creștere a frecvenței plasmei.

În modelul uniparticulă din fizica plasmei, mișcarea unei particule cu sarcina electrică q, respectiv masa m, în prezența unui câmp electromagnetic prescris poate fi descrisă de o girație a particulei în plan perpendicular pe direcția câmpului magnetic, peste care se suprapun drifturi atât în direcție paralelă cât și în direcție perpendiculară pe direcția câmpului magnetic. Frecvența unghiulară de girație poartă numele de **frecvență Larmor** ω_L și este dată de relația:

$$\omega_L = \frac{qB}{m}$$

unde B este modulul inducției câmpului magnetic.

Raza de girație a particulei în plan perpendicular pe direcția câmpului magnetic, numită **rază Larmor** r_L, este dată de expresia:

$$r_L = \frac{mv_\perp}{qB}$$

n care: $v_\perp$ este componenta perpendiculară a vitezei particulei.

Pentru ca un sistem de particule neutre, particule încărcate cu sarcină electrică, cuante de radiație și câmpuri electromagnetice să poată fi numit plasmă, trebuie să îndeplinească următoarele condiții:

- densitatea purtătorilor de sarcină electrică negativă N_- trebuie să fie egală cu densitatea purtătorilor de sarcină electrică pozitivă N_+. Aceasta este condiția de *cvasineutralitate macroscopică*: $N_- \cong N_+ \equiv N_0$

- dimensiunile caracteristice ale volumului plasmei L trebuie să fie mult mai mari decât lungimea *Debye* λ_D: $L \gg \lambda_D$

- timpii caracteristici fenomenelor studiate în plasmă τ trebuie să fie mult mai mari decât inversul frecvenței plasmei v_P: $\tau \gg \frac{1}{v_P}$

- numărul de particlue din sfera Debye N_D trebuie să fie mult mai mare ca unitatea: $N_D \gg 1$

Funcţie de dimensiunile caracteristice ale volumului plasmei l, lungimea *Debye* λ_D, drumul liber mediu de ciocnire λ_C, şi raza Larmor r_L, distingem trei tipuri generale de plasme:

- *plasme rarefiate* sunt plasmele care îndeplinesc următoarele condiţii:

$$l >> \lambda_D,$$
$$l < \lambda_C.$$

Aceste plasme mai sunt cunoscute sub numele de plasme fără ciocniri

- *plasme medii* sunt plasmele care îndeplinesc următoarele condiţii:

$$l >> \lambda_D,$$

$$l >> \lambda_C.$$

- *plasme dense* sunt plasmele care îndeplinesc următoarele condiţii:

$$l >> \lambda_D,$$

$$r_L^e >> \lambda_c^e,$$

$$r_L^i > \lambda_c^i.$$

Aceste plasme pot fi considerate ca reprezentând un mediu continuu.

Analiza parametrica

Vom folosi *Lungimea Debye:*

$$\lambda_D^e = \sqrt{\frac{\varepsilon_0 kT_e}{e^2 N_0}}$$

Pentru calcularea lungimii *Landau* :

$$\lambda_L = \frac{e^2}{6\pi\varepsilon_0 kT_e}$$

Frecventa plasmei este :

$$v_P = \frac{1}{2\pi}\left(\frac{e^2 N_0}{\varepsilon_0 m_e}\right)^{1/2}$$

Conditia de plasma: $N_0 \ll 10^{11} T_e^3$

Conditia ca purtatori de sarcina sa dispara ca rezultat al recombinarii de volum: $N_0 \gg 10^{15} T_e^3$

Rezultate: $n_0 = 10^5$

$T_e = 10^4$

$$\lambda_D^e = \sqrt{\frac{\varepsilon_0 k T_e}{e^2 N_0}}$$ $= 14,12$

$$\lambda_L = \frac{e^2}{6\pi\varepsilon_0 k T_e}$$ $= 1,56 * 10^{-11}$

$$v_P = \frac{1}{2\pi}\left(\frac{e^2 N_0}{\varepsilon_0 m_e}\right)^{1/2}$$ $= 9 * 10^3$

Conditia de plasma

$$N_0 \ll 10^{11} T_e^3 = 10^5 \ll 10^{11}(10^4)^3$$

$= 10^5 \ll 10^{23}$

DA este indeplinita Conditia de plasma.

$$N_0 \gg 10^{15} T_e^3 = 10^5 \gg 10^{15}(10^4)^3$$

$= 10^5 \gg 10^{27}$

II.   Quantum Plasmas

1. Introduction

Quantum plasmas have attracted a renewed attention in recent years. The inclusion of quantum terms in the plasma fluid equations – such as quantum diffraction effects, modified equations of state, and spin degrees of freedom – leads to a variety of new physical phenomena. Recent advances include linear and nonlinear quantum ion-acoustic waves in a dense magnetized electron-positron-ion plasma, the formation of vortices in quantum plasmas, the quantum Weibel and filamentation instabilities, the structure of weak shocks in quantum plasmas, the nonlinear theory of a quantum diode in a dense quantum magnetoplasma, quantum ion-acoustic waves in single-walled carbon nanotubes, the many-electron dynamics in nanometric devices such as quantum wells, the parametric study of nonlinear electrostatic waves in two-dimensional quantum dusty plasmas, stimulated scattering instabilities of electromagnetic waves in an ultracold quantum plasma, and the propagation of waves and instabilities in quantum plasmas with spin and magnetization effects.

Plasma can be regarded as quantum when the quantum nature of its particles significantly affects its macroscopic properties. To determine when quantum effects in plasmasare important, their adequate description is needed. As plasma is an ensemble of many particles, the corresponding approach must be based on the appropriate description of a quantum particle.

The description of non-relativistic quantum plasma can be based on either Schrodinger's representation (in which the operators are time-independent, while the time dependence of physical quantities of the system is defined by the corresponding time dependence of the system's wave function or density matrix) or Heisenberg's representation (in which the time dependence is transferred from the wave functions to the operators). Most of quantum plasma models that are commonly used now use the Schrodinger's representation; the quantum plasma state is described either by wave functions of separate particles (the so-called multistream model), or by the density matrix, or by the Wigner function defined in terms of the density matrix in coordinate representation, or – and this approach has become popular recently – by a set of the so-called quantum hydrodynamics equations.

Naturally, simplifying assumptions are made in all these models (which thus lead to limitations of their applicability), which one should take into account when analyzing results obtained from them. However, concrete applicability limits of results obtained from a particular model are not always stated explicitly (this especially concerns the widely used model of quantum hydrodynamics), which can lead to their incorrect interpretation. This has recently been pointed out, for example, by Melrose and Mushtaq as well as by Kuzelevand Rukhadze.

With the recent rapid increase in the number of publications on quantum plasmas, the lack of detailed analysis of the made assumptions and the associated limitations for the most common quantum plasma models becomes increasingly obvious, and therefore it is useful to provide such analysis. Beyond this, there is an important problem of macroscopic observability of quantum phenomena in plasmas; this problem is also connected with the question of when (and which) quantum phenomena are important in quantum plasmas.

The answer to this question of course depends on the models and approximations used to describe the quantum plasma. In this paper, we provide a detailed analysis of the quantum hydrodynamics model, and study the kinetic features of analytical properties of the linear dielectric response function in isotropic unmagnetized quantum plasma. In doing this, we highlight the most important, in our view, fundamental problems associated with the linear response of quantum plasma, which require further investigation.

2. Properties of Quantum Plasma

We here summarize some of the properties that distinct quantum plasmas from classical plasmas. While classical plasmas are characterized by low density and high temperature, quantum plasmas have high density and low temperature. The quantum N-body problem is governed by the Schr¨odinger equation for the N-particle wave function $\psi(q_1, q_2,..., q_N, t)$ where $q_j = (r_j, s_j)$ is the coordinate(space, spin) of particle j. For identical Fermions, the equilibrium N-particle wave function is given by the Slater determinant.

$$\psi(q_1, q_2, \ldots, q_N, t) = \frac{1}{\sqrt{N!}}$$
$$\times \begin{vmatrix} \psi_1(q_1,t) & \psi_2(q_1,t) & \cdots & \psi_N(q_1,t) \\ \psi_1(q_2,t) & \psi_2(q_2,t) & \cdots & \psi_N(q_2,t) \\ \vdots & \vdots & \ddots & \vdots \\ \psi_1(q_N,t) & \psi_2(q_N,t) & \cdots & \psi_N(q_N,t) \end{vmatrix},$$

(1)

which is anti-symmetric under odd numbers of permutations. Hence, ψ vanishes if two rows are identical, which is an expression of the Pauli exclusion principle that two identical Fermions cannot occupy the same state. Example (N = 2): $\psi(q_1, q_2, t) = \frac{1}{\sqrt{2}}[\psi_1(q_1, t)\psi_2(q_2, t) - \psi_1(q_2, t)\psi_2(q_1, t)]$ so that $\psi(q_2, q_1, t) = -\psi(q_1, q_2, t)$ and $\psi(q_1, q_1, t) = 0$. Due to the Pauli exclusion principle, all electrons are not permitted to occupy the lowest energy state, and in the ultra-cold limit when all energy states up to the Fermi energy level are occupied by electrons, there is still a quantum-statistical pressure determined by the Fermi pressure.

Quantum effects start playing a significant role when the de Broglie wavelength is similar to or larger than the average interparticle distance $n^{-1/3}$, i.e. when

$$n\lambda_b^3 \geq 1 \qquad (2)$$

or, equivalently, the temperature is comparable or lower than the Fermi temperature $T_F = E_F/k_B$, where

$$E_F = \frac{\hbar^2}{2m}(3\pi^2)^{2/3}(n\lambda_B^3)^{2/3} \geq 1 \qquad (3)$$

is the Fermi energy for electrons, so that

$$\chi = \frac{T_F}{T} = \frac{1}{2}(3\pi^2)^{\frac{2}{3}}(n\lambda_B^3)^{2/3} \geq 1 \ (4)$$

When the temperature approaches T_F, one can show using density matrix formalism that the equilibriumelectron distribution changes from Maxwell–Boltzmann $\propto \exp(-E/K_BT)$ to the Fermi–Dirac statistics $\propto [\exp((E + \mu)/K_BT) + 1]^{-1}$. For an ultracold plasma, the Fermi screening scalelength

$$\lambda_F = \frac{V_F}{\omega_P} \ (5)$$

is the quantum analogue of the Debye radius, where the Fermi speed

$$V_F = (2E_F/m)^{1/2} = \frac{\hbar}{m}(3\pi^2 n)^{1/3} (6)$$

is the speed of an electron at the Fermi surface. The quantum coupling parameter

$$G_q = \frac{E_{int}}{E_F} \sim (\frac{1}{n\lambda_F^3})^{2/3} \sim (\frac{\hbar\omega_p}{E_F})^2 (7)$$

is analogous to the classical one when $\lambda_F \rightarrow \lambda_D$.

The quantum analogue to the Vlasov-Poisson systemis the Wigner-Poisson model

$$\frac{\partial f}{\partial t} + v \cdot \nabla f = -\frac{iem_e^3}{(2\pi)^3\hbar^4} \iint e^{im_e(v-v')\cdot\frac{\lambda}{\hbar}} \times [\phi\left(x + \frac{\lambda}{2}, t\right) - \phi(x - \frac{\lambda}{2}, t)]f(x, v', t)d^3\lambda d^3v'(8)$$

and

$$\nabla^2\phi = 4\pi e(\int f d^3v - n_0). \qquad (9)$$

Note that the Wigner equation converges to the Vlasovequation for classical particles when $\hbar \rightarrow 0$

$$\frac{\partial f}{\partial f} + v \cdot \nabla f = -\frac{e}{m_e}\nabla\phi \cdot \frac{\partial f}{\partial v} \ (10)$$

We take the moments of the Wigner equation and obtain the quantum-electron fluid equations

$$\frac{\partial n}{\partial t} + \nabla \cdot (nu) = 0, \qquad (11)$$

$$m\left(\frac{\partial u}{\partial t} + u \cdot \nabla u\right) = e\nabla\phi - \frac{1}{n}\nabla P + F_Q, \qquad (12)$$

where ϕ is determined from $\nabla^2\phi = 4\pi e(n - n_0)$, and for the degenerate Fermi-Dirac distributed plasma one has (up to constants of order unity) the quantum statistical pressure

$$P = \frac{mV_F^2 n_0}{3}\left(\frac{n}{n_0}\right)^{(D+2)/D}, \qquad (13)$$

where D is the number of degrees of freedom in the system, and the diffraction effects

$$F_Q = \frac{\hbar^2}{2m}\nabla\left(\frac{\nabla^2\sqrt{n}}{\sqrt{n}}\right) \equiv -\nabla_{\phi B}, \qquad (14)$$

where ϕB is the Bohm potential. Linearization of the NLS-Poisson Equations yields the frequency of EPOs

$$\omega_k = \left(\omega_{pe}^2 + k^2 V_{TF}^2 + \frac{\hbar^2 k^4}{4m_e^2}\right)^{1/2}, \quad (15)$$

where

$$V_{TF} = \sqrt{\frac{k_B T_{Fe}}{m_e}}. \qquad (16)$$

One can identify two distinct dispersive effects: one long wavelength regime, $V_{TF} \gg \hbar k/2m_e$, and one short wavelength regime, $V_{TF} \ll \hbar k/2m_e$, separated by the critical wavenumber

$$k_{crit} = \frac{2\pi}{\lambda_{crit}} = \frac{\pi\hbar}{m_e V_{TF}} \sim n^{-1/3}. \quad (17)$$

Similar results have been obtained by Bohm and Pines, see Refs. Quantum diffraction effects have recently been observed in experimental observations of electrostatic oscillations in quantum plasmas. By introducing the effective wave function

$$\psi(r,t) = \sqrt{n(r,t)}\exp iS(r,t)/\hbar), \qquad (18)$$

where S is defined according to mu $= \nabla S$ and $n = |\psi|^2$, one can show that the QHD equations are equivalent to the effective NLS-Poisson system

$$i\hbar\frac{\partial\psi}{\partial\psi} + \frac{\hbar^2}{2m}\nabla^2\psi + e\phi\psi - \frac{mV_F^2}{2n_0^2}|\psi|^{\frac{4}{D}}\psi = 0, \qquad (19)$$

and

$$\nabla^2 \phi = 4\pi e(|\psi^2| - n_0). \qquad (20)$$

The effective NLS equation (19) captures the two main properties of a quantumplasma, namely the quantum statistical pressure and the quantum diffraction effects, and is coupled self-consistently to the electrostatic potential given by the Poisson equation (20). We note that one-dimensional version of Eq. (19) without the φ-termhas also been used to describe the behaviour of a Bose-Einstein condensate. We will give two examples in the next sections where this formalism has been used to analyze nonlinear effects in a quantum plasma.

3. Basic Methods of Description of Quantum Plasmas

As in the case of classical plasmas, the most complete description of quantum plasma as a system of many interacting particles is a completely hopeless task. In case of quantum plasma this task is in a sense even more hopeless than in case of classical plasma, not only because it is impossible to solve the Schrodinger's equation for the N-particle wavefunction of the system, but also because of the lack of such wavefunction for a macroscopic system that interacts, however weakly, with its environment. Yet the problem can be significantly simplified by assuming that the plasma is nearly ideal, i.e., that the two- and higher-order correlations between its particles can be neglected. If this is the case, then the plasma can be considered as a collection of quantum particles that interact only via their collective field. As mentioned above, the most commonly used now are the following models (which all in fact use the assumption of ideal plasma):
- (i)   the quantum analog of the multistream model,
- (ii)   the kinetic model based on the Wigner equation for the density of quasi-probability of particle distribution in coordinates and momenta, and, finally,
- (iii)   the quantum hydrodynamics model.

 All of these models, in one way or another, are based on the Schr̈odigner's equations for the wavefunctions of plasma particles, and therefore are non-relativistic; hence they can only be used for describing non-relativistic ideal plasmas and, strictly speaking, for describing plasma oscillations with small (non-relativistic) phase velocities ω/k ≪ c (here ω and k are frequency and wavenumber of the oscillations, respectively, and c is the speed of light). We should note, however, that more general relativistic models of "quantum plasmadynamics" appeared recently; we expect that these models will be more widely used in the future, due to their logically consistent description of both quantum particles and quantized fields. However, here we will only consider the non-relativistic models, as they are the most widely used in recent literature on quantum plasmas, probably owing to their relative simplicity.
Description of quantum plasma should be started with the models of Hartree and Hartree-Fock, in which N independent Schrodinger equations for N plasma particles are coupled via the

average self-consistent field (in Hartree-Fock's model the correction due to exchange interactions is also taken into account). The Hartree and Hartree-Fock approximations for quantum plasmas are analogous to the self-consistent field approximation in description of classical plasmas, and they form a basis for kinetic and hydrodynamic models of quantum plasmas. Therefore it is important for further considerations to write down their main assumptions.

Main assumptions of the Hartree and Hartree-Fock models

1. Plasma particles interact only through average classical (i.e., not quantized) collective fields.

2. Plasma is ideal, $\Gamma_q = U_{int}/\epsilon_F = e^2 n^{1/3}/\epsilon_F \sim (\hbar\omega_p/\epsilon_F)^2 \ll 1$, where $\epsilon_F = (\hbar^2/2m)(3\pi^2 n)^{2/3}$ is the Fermi energy of electrons, $\omega_p = (4\pi e^2 n/m)^{1/2}$ is electron plasma frequency, and e, m and n are charge, mass, and number density of electrons. We should note that for the electron gas in metals the condition $\Gamma_q \ll 1$ is in general not satisfied: in metals we have $\Gamma_q \sim 1$.

3. Non-relativistic approximation is used; see the discussion after Eq.

Kinetic models of Wigner-Poisson and Wigner-Maxwell These models are based on the Wigner equation describing time evolution of the Wigner function [4], which is coupled with either Poisson's equation or Maxwell's equations describing the self-consistent collective electrostatic and electromagnetic field, respectively. The Wigner function describes quasidensity of quantum particle probability distribution in coordinate-momentum phase space (we call it quasi-density because the Wigner function can attain negative values, due to noncommutativity of position and momentum operators in quantum mechanics, i.e., due to uncertainty principle). The Wigner function f(q,P, t) is defined from the density matrix $\rho(q,q',t)$ of plasma in coordinate representation as follows:

$$f(q,P) = \frac{1}{(2\pi)^N} \int d\vec{\tau} e^{-i\vec{\tau}P} \rho(q - \frac{1}{2}\hbar\vec{\tau}, q + \frac{1}{2}\hbar\vec{\tau}), \qquad (21)$$

where q and P are canonically conjugated generalized coordinate and momentum, N is the number of components of P (and/or of q) and corresponds to the number of coordinates of 5a particle (N = 3 in a 3-dimensional system). The Wigner function is normalized so that

$$n(q) = \int f(q,P)dP, \qquad (22)$$

where n(q) is the number density of plasma particles. The Wigner equation, which describes evolution of the Wigner function, follows from the evolution equation for the density matrix in coordinate representation, and has the following form:

$$\frac{\partial f(q,P)}{\partial t} = \frac{1}{(2\pi)^N} \frac{i}{\hbar} \int \ldots \int d\vec{\tau} dk d\vec{\eta} dr e^{i[\vec{\tau}(\vec{\eta}-P)+k(r-q)]} f(r,\vec{\eta}) \times [H\left(\vec{\eta}+\frac{1}{2}\hbar k, r+\frac{1}{2}\hbar\vec{\tau}\right)],$$

(23)

where H is the Hamiltonian of the system.

Main assumptions of Wigner-Poisson and Wigner-Maxwell models

1. Plasma is ideal, $\Gamma_q = U_{int}/\epsilon_F = e^2 n^{1/3}/\epsilon_F \sim (\hbar\omega_p/\epsilon_F)^2 \ll 1$. As noted above, this condition is not satisfied for electron gas in metals, where $\Gamma_q \sim 1$. Type equation here.

2. Plasma particles interact only via average collective fields that are described by Maxwell's equations (i.e., classical electrodynamics is assumed for the fields).

3. Collisions between quantum particles are not taken into account (the models are collisionless).

4. Non-relativistic approximation is used.

5. Usually, spin of particles (as well as exchange interactions) are not taken into account. However, the effect of spin can still be accounted for in the workframe of non-relativistic Wigner-Maxwell model by introducing the spin distribution function and writing the corresponding kinetic equation for this function; this has been done, for example, by Silin and Rukhadze.

4. Multistream model

This model is based on the Hartree approximation of plasma particles interacting via self-consistent collective fields only. Plasma is considered as a collection of weakly correlated "cold beams" formed by groups of particles with the same momenta; these beams are assumed to interact only through their collective fields. Using linearized equations of "cold hydrodynamics" for each of these groups of particles (beams), their current density and the corresponding dielectric permittivity tensor are calculated. Then adding up the contributions of all groups of plasma particles with the corresponding "weight functions", i.e., averaging these contributions over plasma equilibrium distribution function f0(p), one obtains the dielectric permittivity tensor of the whole plasma (see Sec. IV for details of this procedure). This procedure is equivalent to calculating the dielectric permittivity tensor directly from the Wigner equation (5), since the latter is based on the same assumption of weakly correlated particles interacting only via their collective fields.

Main assumptions of the multistream model

Same as for kinetic models based on the Wigner equation (see above).

III. Quarck-Gluon Plasma

1. Why this is referred to as "plasma"

A plasma is matter in which charges are screened due to the presence of other mobile charges; for example: Coulomb's Law is modified to yield a distance-dependent charge. In a QGP, the color charge of the quarks and gluons is screened. The QGP has other analogies with a normal plasma. There are also dissimilarities because the color charge is non-abelian, whereas the electric charge is abelian. Outside a finite volume of QGP the color electric field is not screened, so that volume of QGP must still be color-neutral. It will therefore, like a nucleus, have integer electric charge.

2. General introduction

Quark–gluon plasma is a state of matter in which the elementary particles that make up the hadrons of baryonic matter are freed of their strong attraction for one another under extremely high energy densities. These particles are the quarks and gluons that compose baryonic matter. In normal matter quarks are confined; in the QGP quarks are deconfined. In classical QCD quarks are the Fermionic components of mesons and baryons while the gluons are considered the Bosonic components of such particles. The gluons are the force carriers, or bosons, of the QCD color force, while the quarks by themselves are their Fermionic matter counterparts.

Although the experimental high temperatures and densities predicted as producing a quark-gluon plasma have been realized in the laboratory, the resulting matter does not behave as a quasi-ideal state of free quarks and gluons, but, rather, as an almost perfect dense fluid. Actually, the fact that the quark-gluon plasma will not yet be "free" at temperatures realized at present accelerators was predicted in 1984 as a consequence of the remnant effects of confinement.
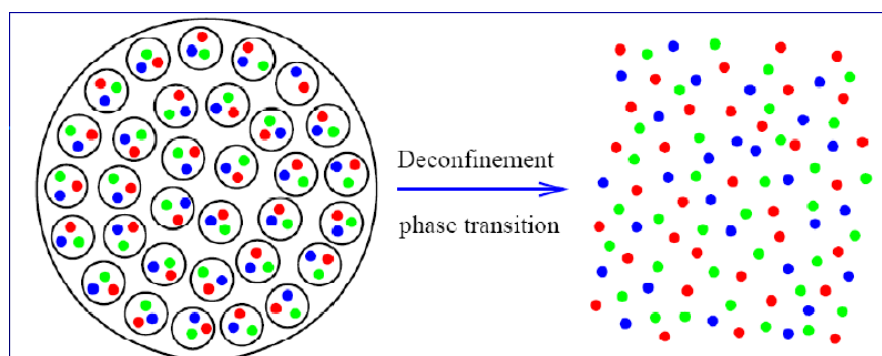
3. Short description

Quark-gluon plasma appears in heavy-ion(nucleus-nucleus) collisions: protons and neutrons decays into their constituents to form this type of plasma.
It is characterized by:

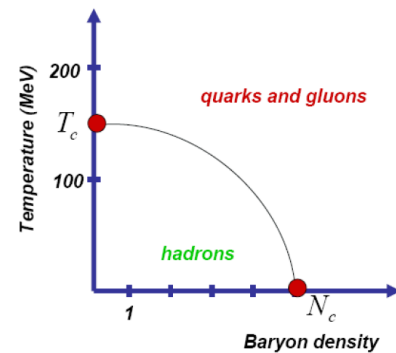

- o   Critical baryon density:

$$\rho_0 = 0.125 GeV / fm^3 = 2.2 \cdot 10^{17} kg / m^3 \quad \rho_C = 10\rho_0;$$

- o   Critical temperature:
   T_C=150-200 MeV=(1.8-2.4)x10^{12} K

- o   Life-time of QGP:
   $\tau = 5 - 10 fm / c$

High energy quarks and gluons propagating through quark-gluon plasma suffer differential energy loss via elastic scattering from quanta in the plasma. This mechanism is very similar in structure to ionization loss of charged particles in ordinary matter. The dE/dx is roughly proportional to the square of the plasma temperature. For hadron-hadron collisions with high associated multiplicity and with transverse energy dET/dy in excess of 10 GeV per unit rapidity, it is possible that quark-gluon plasma is produced in the collision.
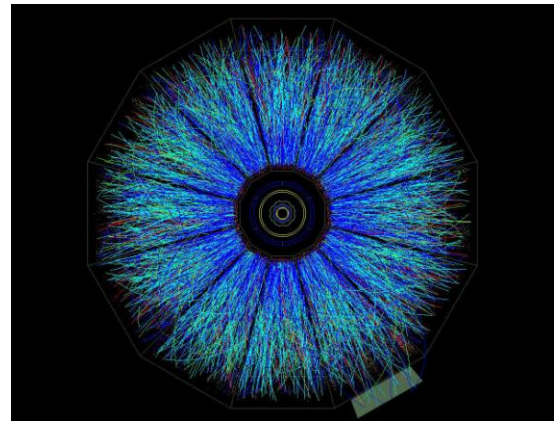
Collisional energy loss of a quark with energy E in a QGP:

$$\frac{dE}{dx} = -\frac{4\pi}{3}(1 + \frac{N_f}{6})\alpha_s^2 T^2 \ln\frac{E}{\alpha_s T}$$

A quark–gluon plasma (QGP) or quark soup is a phase of quantum chromodynamics (QCD) which exists at extremely high temperature and/or density. This phase consists of asymptotically free quarks and gluons, which are several of the basic building blocks of matter. Experiments at CERN's Super Proton Synchrotron (SPS) first tried to create the QGP in the 1980s and 1990s: the results led CERN to announce indirect evidence for a "new state of matter" in 2000. Current experiments (2011) at the Brookhaven National Laboratory's Relativistic Heavy Ion Collider(RHIC) at Long Island (NY, USA) and, respectively, at CERN's recent LHC collider at

Geneva (Switzerland) are continuing this effort, by smashing relativistically accelerated gold atoms rsp. lead atoms onto each other .

QGP cannot be observed directly: discovery of quark-gluon plasma is made by comparison of theoretical predictions for signatures with experimental data.

As already mentioned, three new experiments running on CERN's Large Hadron Collider (LHC), on the spectrometersALICE, ATLAS and CMS, will continue studying properties of QGP. Starting in November 2010, CERN temporarily ceased colliding protons, and began colliding lead Ions for the ALICE experiment. They were looking to create a QGP and were expected to stop December 6, colliding again protons in January.Within the first week of colliding these lead ions, the LHC appears to have created multiple quark-gluon plasmas
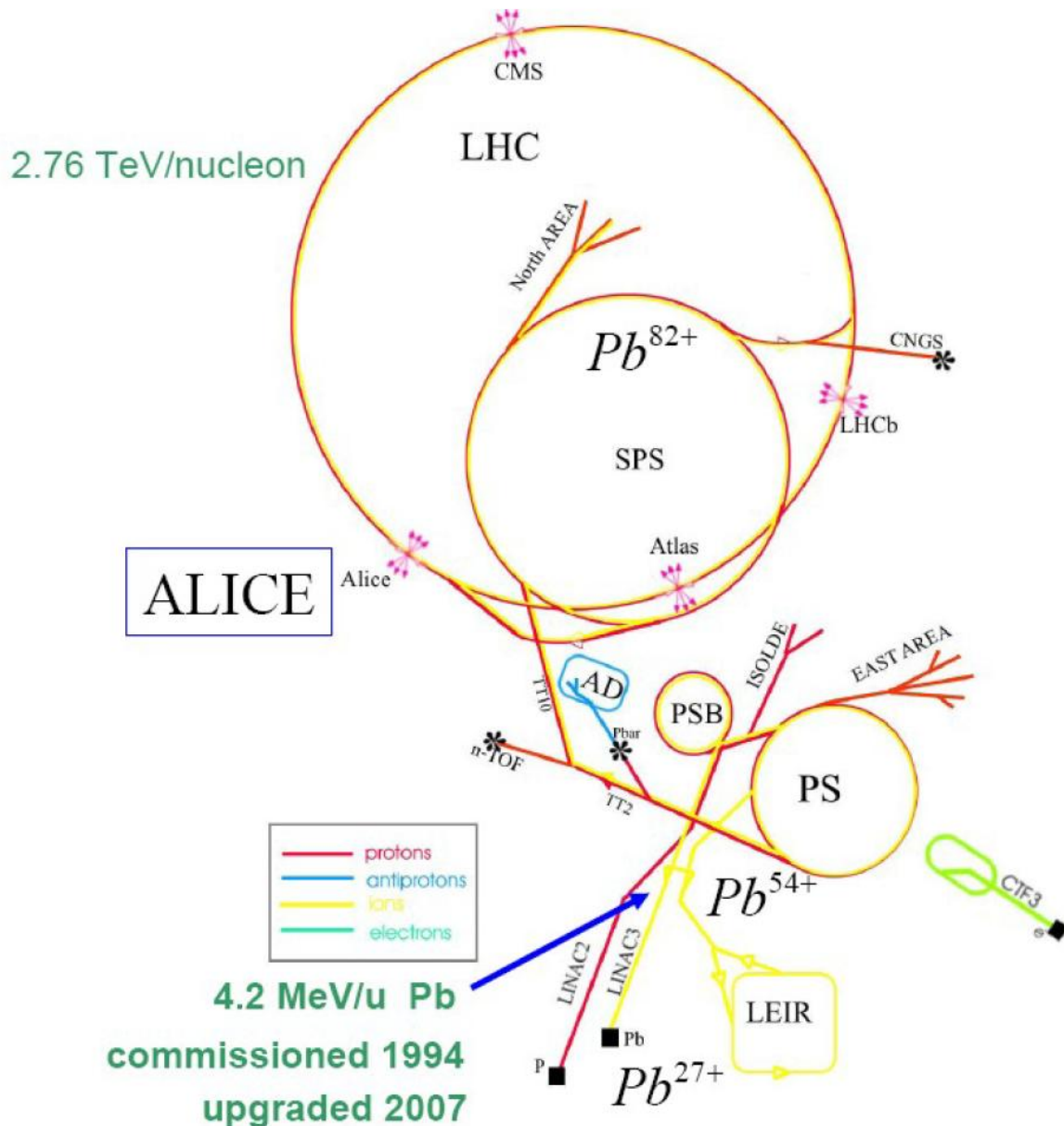
withtemperatures in the tens of trillions of degrees.

4. The Large Hadron Collider

The Large Hadron Collider (LHC)[1] accelerates protons in a 27 km long tunnel located at the European Organization for Nuclear Research (CERN) in Geneva, Switzerland. The LHC will also accelerate lead ions to make them collide at the highest energy ever.

The acceleration process starts in Linac 2 for protons and Linac 3 for lead ions. The protons accelerated in Linac 2 are injected into a Proton Synchrotron Booster with an energy of 50 MeV. In the synchrotron, protons reach an energy of 1.4 GeV. The Super Proton Synchrotron (SPS) has been modified to deliver a high-brightness proton beam required by the LHC. The SPS takes 26 GeV protons from the Proton Synchrotron (PS) and brings them to 450 GeV before extraction.

The Linac 3 produces 4.2 MeV/u lead ions. Linac 3 was commissioned in 1994 by an international collaboration and upgraded in 2007 for the LHC. The Low Energy Ion Ring (LEIR) is used as a storage and cooler unit providing ions to the (PS) with an energy of 72 MeV/nucleon. Ions will be further accelerated by the PS and the SPS before they are injected into the LHC where they reach an energy of 2.76 TeV/nucleon.

The LHC consists of 1232 superconducting dipole magnets with double aperture that operate at up to 9 Tesla magnetic field. The accelerator also includes more than 500 quadrupole magnets and more than 4000 corrector magnets of many types.
Ions are obtained from purified lead that is heated to 550 C. The lead vapour is then ionized with an electric current that produces various charge states. The Pb ions are then selected with magnetic fields. This process takes place in an Electron Cyclotron Resonance (ECR) source
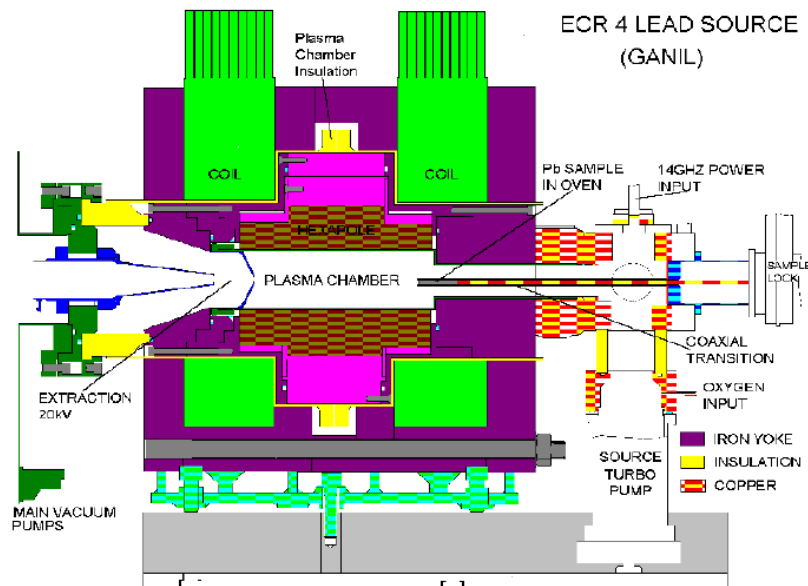
The ECR lead source is equipped with an hexapole permanent magnet. The plasma chamber is immersed in a solenoidal magnetic field. Pulsed beam currents produce Pb ions that are then extracted to the Linac.

After acceleration, the lead ions go through a carbon foil that strips them to Pb , which are accumulated in the Low Energy Ion Ring (LEIR). LEIR is a circular machine which transforms the long pulses of Linac 3 into high-density bunches needed by the LHC. LEIR injects bunches of ions to the PS.

At the SPS, ions go once more through a thin aluminium foil which strips them to Pb. The thickness of the stripper foil has to be chosen carefully to reduce contamination of lower charge states and keep emittance low. Foils of 0.5 to 1 mm thickness have been studied. In this way, fully stripped lead ions are obtained for the LHC.

The total cross-section of proton–proton interaction at 7 TeV could be inferred from hadronic cross-section measurements at lower energy [2]. It would be around 110 mbarn and correspond to about 60 mbarn of inelastic-scattering cross-section. The accelerator, at its design level, will reach a luminosity of $10^{34} s^{-1} cm^{-1}$ which means that the interaction rate will be

$$Rate = 10^{34}(1/cm^2 s) * 60 * 10^{-3} barn * 10^{-24} cm^2/barn = 600 * 10^6 \text{collisions/s}$$

A 25 ns interval between bunches gives a 40 MHz crossing rate. On average 19 inelastic events will occur each time bunches cross. Since there will be gaps in the beam structure, an average crossing rate of 31.6 MHz will be reached. Detectors at the LHC must be designed to cope with these frequencies. However, ALICE will run at a modest 300 kHz interaction rate in proton–proton mode and 10 kHz in Pb–Pb.
During autumn 2009, bunches of protons will be injected into the LHC ring. During the start-up phase, first collisions with protons at 3.5 TeV will take place. An increase of the proton beam energy in a second phase is foreseen. By the end of the run with protons in year 2010, lead-ion collisions will be produced.
The ALICE experiment is ready to take data on all the phases of the accelerator operation.

5. The ALICE experiment

The ALICE experiment has been designed to observe the transition of ordinary matter into a plasma of quarks and gluons [3]. At the energies achieved by the LHC, the density, the size, and the lifetime of the excited quark matter will be high enough to allow a careful investigation of the properties of this new state of matter. The temperature will exceed by far the critical value predicted for the transition to take place.

ALICE has been optimized to study global event features. The number of colliding nucleons will provide information on the energy density achieved. The measurement of elliptic flow patterns will provide information about thermalization on the partonic level and the equation of state of the system in the high-density phase. Particle ratios in the final state are connected to chemical equilibration and provide a landmark on the trajectory of the system in the phase diagram. The spacetime evolution of the system can be investigated via particle interferometry, complemented by the study of resonaces. Moreover, important information about the system properties can be obtained by the study of hard probes, which will be produced abundantly at the LHC. Deconfinement may be reflected in the abundancies of J/ψ and Upsilon. The study of jet production on an event-by-event basis will allow one to investigate the transport properties of hard-scattered partons in the medium, which are expected to be strongly modified if a quark–gluon plasma is formed.

ALICE is also well suited for studies of proton–proton and photon–photon reactions. Photon–photon reactions include QED and QCD processes that go from lepton-pair to hadron and jet production. As for proton–proton interactions, diffractive physics would be an exciting area of research.

The ALICE detector will have a tracking system over a wide range of transverse momentum which goes from 100 MeV/c to 100 GeV/c as well as particle identification able to separate pions, kaons, protons, muons, electrons, and photons.

A longitudinal view of the ALICE detector:
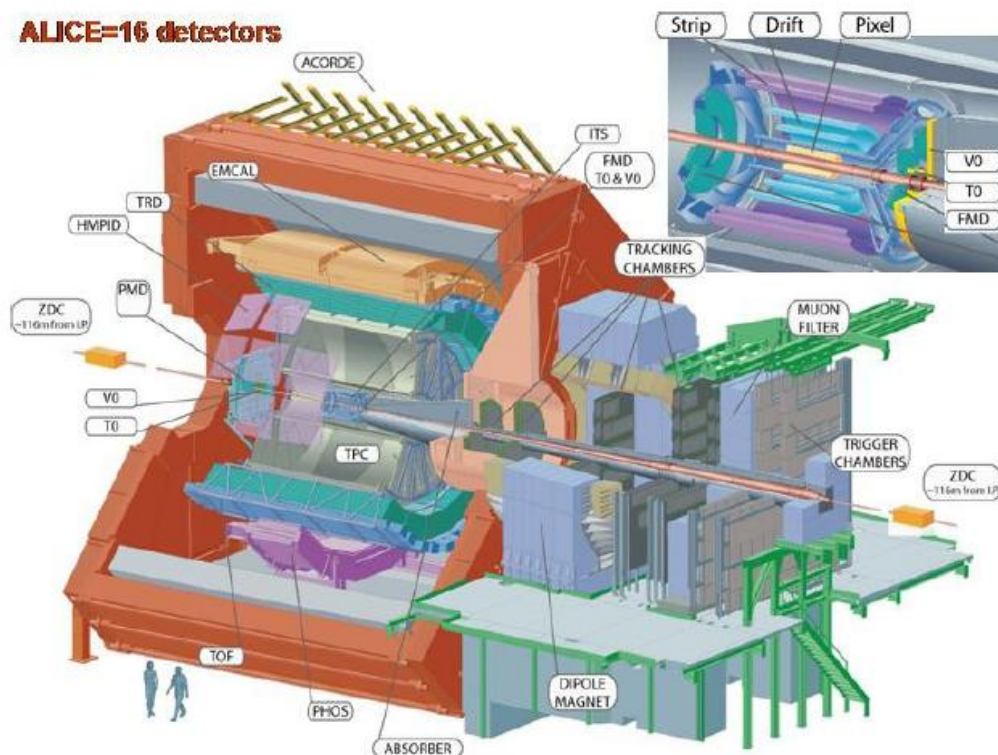
In the forward direction a set of tracking chambers inside a dipole magnet will measure muons. An absorber will stop all the products of the interaction except for the muons which travel across and reach the tracking chambers that form the muon arm.

The central part of the ALICE detector is located inside a solenoid that provides a magnetic field of 0.5 T. The central tracking and particle identification system cover - $0.9 < \eta < 0.9$.

Electrons and photons are measured in the central region: photons will be measured in PHOS, a high-resolution calorimeter 5 m below the interaction point. The PHOS is built from $PBWO_4$ crystals which have a high light output.

The track measurement is performed with a set of six barrels of silicon detectors and a large Time Projection Chamber (TPC). The TPC has an effective volume of 88 m^3. It is the largest TPC ever built. These detectors will make available information on the energy loss allowing particle identification too. In addition to this, a Transition Radiation Detector (TRD) and a Time-of-Flight system will provide excellent particle separation at intermediate momentum. The Time-of-Flight system (TOF) uses Multi-gap Resistive Plate Chambers (MRPCs) with a total of 160 000 readout channels. A Ring Imaging Cherenkov detector will extend the particle identification capability to higher momentum particles. It covers 15% of the acceptance in the central area and will separate pions from kaons with momenta up to 3 GeV/c and kaons from protons with momenta up to 5 GeV/c.

A Forward Multiplicity Detector (FMD) consisting of silicon strip detectors and a Zero Degree Calorimeter (ZDC) will cover the very forward region providing information on the charge multiplicity and energy flow. A honeycomb proportional counter for photon multiplicity (PMD) measurements is located in the forward direction on one side of the ALICE detector.

The trigger system is complemented by a high level trigger (HLT) system which makes use of a computer farm to select events after read-out. In addition, the HLT system provides a data quality monitoring.

The V0 system is formed by two scintillation counters on each side of the interaction point. The system will be used as the main interaction trigger. In the top of the magnet, A Cosmic Ray Detector (ACORDE) will signal the arrival of cosmic muons.

IV. White Dwarfs

1. Short History of White Dwarfs

First observations on white dwarfs began with Friedrich Wilhelm Bessel in 1834. At that time, Bessel noticed that the motion of Sirius, the brightest star in the night sky, was irregular. The star appeared somehow to wobble, to oscillate, thus suggesting that Sirius is one component star, but of binary system. After 10 years of observation (1834 - 1844), Bessel concluded that Sirius and the unseen pair are revolving one another with a period of 50 years. However, it was not until January 31st in the year of 1862 that Alvan Graham Clark imaged for the first time the blurred companion (Sirius B) using a 18 inch telescope for the Dearborn Observatory.

Sirius A and Sirius B have a luminosity ratio of about 10^4; nevertheless the colours of the two seemed to be quite similar. Firstly, similar colours indicate similar temperatures, and therefore it was estimated that the radius of Sirius B was about 100 times smaller than Sirius A (since $L = 4\pi R^2 \sigma T^4$). This fact was confirmed in 1915 by Walter Sydney Adams when he measured the spectrum of Sirius B and confirmed that it was a blue star.

The first white dwarf had been discovered, an object as massive as the Sun, yet only as large as the Earth. Adams continued the research and by 1925 measured a gravitational redshift from Sirius B, confirming the very dense nature of this object (about 1.000.000 g/ cm^3). This proof was also a successful test to Einstein's theory of relativity. This then spurred a number of very important theoretical advancements to try and understand these objects, and in particular to understand the relativistic electron degeneracy equation of state (see e.g., Chandrasekhar 1937).

Since the discovery of the first white dwarf, over 3000 of these objects have been discovered in our Galaxy. The Sloan Digital Sky Survey has already almost doubled this number, and will easily find 10000 new white dwarfs by the end of the Survey (Kleinman et al. 2004). With more new discoveries, the astrophysical uses of these objects continue to grow.

2. Introduction

The beauty of a white dwarf lies in its demonstration that a system at the length scale of Earth's radius and the mass scale of the sun can be inherently quantum. In a remarkable historical coincidence, the Schrodinger equation was formulated in the same year that the astrophysicist William A. Fowler (1926) wrote that "a star was like a giant molecule in its ground state" supported against gravitational collapse by degeneracy pressure. Since then, this comparison has inspired a rich body of literature adapting the techniques of solving for the electronic structure of atoms and molecules to the study of degenerate compact stars such as white dwarfs and neutron stars.

Like that of an atom, the radius of a degenerate star is fully determined by the number of nucleons and electrons that it contains. One might ask why atomic nuclei are only stable up to nucleon numbers Z on the order of 10^2 whereas white dwarfs have a nucleon number on the order of 10^{57}. The difference is due to the short-range character of the strong nuclear force that supports atomic nuclei against degeneracy pressure, in contrast to the long-range nature of the gravitational force that binds together degenerate stars [2]. The stability criteria for non-relativistic white dwarfs was derived by E.C. Stoner in 1930 [3], and a mass limit for ultra-relativistic white dwarfs was discovered by Chandrasekhar in 1931 [4].

The purpose of this study is to give physical motivations for the use of Thomas-Fermi theory in studying white dwarfs and present extensions to the calculations of Stoner and Chandrasekhar using the Thomas-Fermi semi classical approximation, originally developed by Thomas and Fermi in 1927 to estimate the distribution of electrons in an atom [1]. In Section 2, it is summarized Stoner's mass-radius curve calculation and derive the same result purely from the ground state electronic structure of a many-body Hamiltonian that includes gravitational interactions. This method suggests an analogy between white dwarfs and the Bohr atom that is obscured in other derivations that treat gravitational pressure macroscopically.

Section 3 formally introduces Thomas-Fermi theory and presents corrections to the energy of a white dwarf from Coulomb interaction, both non-relativistic and relativistic. Section 4 is a general discussion of the results from Thomas-Fermi calculations applied to the stability criteria of white dwarfs.

At this point, a quick summary of stellar evolution theory is in store. In main sequence stars (like Sun), nuclear fusion of hydrogen to helium supplies the required thermal energy to stall gravitational contraction of a star, enabling it to attain a quasi-hydrostatic equilibrium. As the star advances in age, a further sequence of nuclear fusion reactions gets activated in its core - helium burning to carbon and oxygen, carbon burning to sodium and magnesium and so on, if the star is massive enough, till the formation of iron-rich core. Iron nucleus being the most stable one, subsequent nuclear burning cease to take place. As the core cools, it collapses under its own weight, till the electron density becomes so high that electron degeneracy pressure prevents further contraction.

Degeneracy pressure is a consequence of quantum statistics in extremely dense matter. Pauli's exclusion principle (PEP) states that no two identical fermions can have the same state. Electrons, protons, neutrons, neutrinos, etc., being spin half particles, are fermions. According to PEP, in a gravitationally bound system like the iron-rich core of an evolved star, all the electrons cannot occupy the lowest energy level (unlike, what happens to identical bosons in Bose-Einstein condensates, e.g. He-4 superfluid). So, the energy levels are filled up with two electrons (one

with spin up state and the other with spin down) per orbital, as demanded by the PEP. Hence, more the density of electrons, higher is the energy level that gets to be occupied.

Gravitational shrinking of such a dense core leads to an increase in electron density, thereby facing a resistance since the contraction implies putting electrons at higher energy levels. Therefore, in such a degenerate system, gravitational collapse instead of lowering the energy of the star tends to increase it. The resulting pressure against shrinking, arising out of PEP in such electron-rich dense matter is called electron degeneracy pressure (EDP).

A white dwarf is a star that is in hydrostatic equilibrium not because of thermal pressure but due to the EDP that counteracts gravitational contraction. Fowler had assumed that electrons are moving non-relativistically inside the core and had shown that the EDP of a white dwarf is proportional to $\rho^{5/3}$, where ρ is the density of the core [1].

3. What are White Dwarfs?

Normal hydrogen burning stars (main-sequence stars) are in a state of hydrostatic equilibrium. The radially inward directed gravitational force is balanced by a thermal pressure exerted from the nuclear reactions occurring in the core of the star. The thermal timescales in a main-sequence star are much greater than dynamical timescales, and therefore the equilibrium holds as long as the star continues to burn hydrogen. However, a star eventually exhausts almost all of its core hydrogen supply and the previously established equilibrium is destroyed. The rate of this hydrogen burning depends almost entirely on the mass of the star, and the subsequent evolution of the star depends on its initial mass. The star will move through many post-main sequence stellar evolutionary stages, such as the sub-giant branch, red giant branch, horizontal branch (or red giant clump in the case of stars with initial masses < 2 $M_\odot$), asymptotic giant branch, planetary nebula stage, and finally the white dwarf stage (in the case of stars with initial masses $\leq$ 7 $M_\odot$). Details of each of these stages can be found in the very thorough review of Chiosi, Bertelli&Bressan (1992). The end product of this chain of events is a "stellar cinder" which fades with time, becoming dimmer by radiating away any remaining stored thermal energy. It is illustrated the locations of these phases and the evolution of a single star which will produce a white dwarf in a Hertzsprung-Russell (HR) diagram in the figure below.

With all of the nuclear fuel exhausted, a white dwarf cannot generate pressure from reactions in the core. Earlier in the evolution, all of the hydrogen (and helium) were burnt and converted into carbon and oxygen. The resulting C/O core cannot support itself from gravitational contraction and therefore gravity compresses the star. The electrons in the core are packed together tighter and tighter. The Pauli exclusion principle only allows two electrons, of different spin, to occupy any energy level and therefore all of the energy levels from the ground level up are filled and the

Figure 3.1: A Hertzsprung-Russell diagram is shown with the main sequence, post main sequence stellar evolutionary phases, and white dwarf cooling phase indicated. The evolution shown is for a 1 $M_\odot$ star
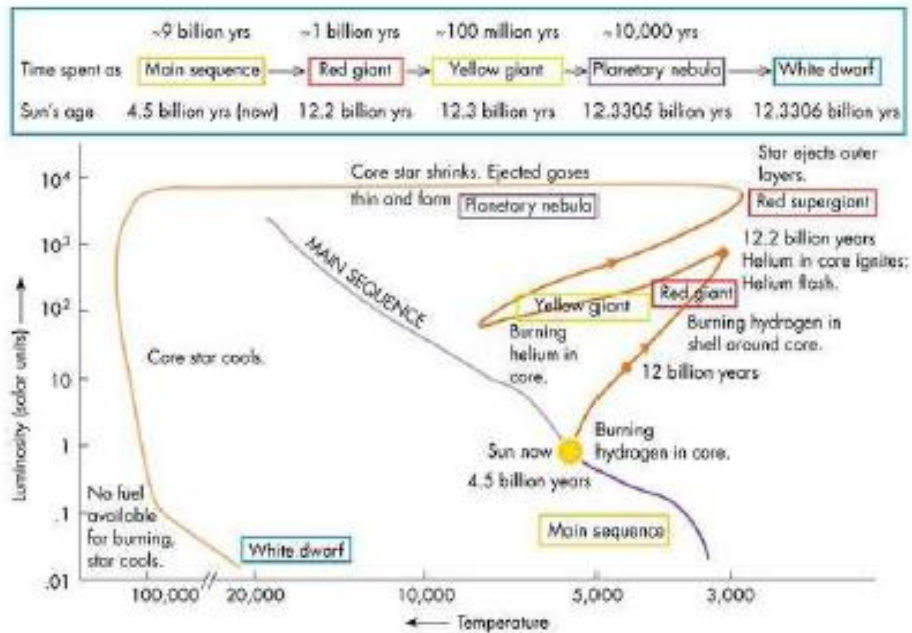
electron gas is said to be degenerate. Invoking the Uncertainty Principle, the space available to each electron, Δx, becomes very small in a white dwarf and therefore the momentum, p, is very large. It is this momentum that generates a degeneracy pressure that supports the star from further collapse. The typical mass of the resulting star is 0.6 $M_\odot$, with a radius of 10^4 km (i.e., $\rho \sim 10^8$ kg/m^3). More detailed properties of white dwarfs can be found in the excellent textbook by Shapiro &Teukolsky (1983).

Several interesting properties exist for degenerate matter. For example, if the mass of the white dwarf is increased, then the electrons are forced to "squeeze" together even more and consequently the radius of the star actually decreases. Therefore, more massive white dwarfs are smaller. Another property of white dwarfs, determined by Chandrasekhar (1937), is that they have a maximum mass. If enough mass is piled onto a white dwarf, the velocity of the electrons continues to increase until they approach the speed of light, at which point degenerate electron pressure can no longer support the star from further collapse. This maximum mass can be easily shown to be ~ 1.4 $M_\odot$, and if reached, results in a type Ia supernova explosion of the star. These explosions occur when massive white dwarfs are members of close binary systems, in which the white dwarf accretes mass from a companion, pushing it over what is now called the "Chandrasekhar limit". Interestingly, an even more extreme type of degeneracy pressure governs the stability of neutron stars, the end products of more massive initial main-sequence stars that do not produce white dwarfs. In that regime, the densities are so high ($\rho \sim 10^{17}$ kg/m^3) that protons and electrons will combine through inverse beta decay to produce neutrons which support the

star through degenerate neutron pressure. Observationally, most neutron stars are found to have a mass of about 1.5 $M_\odot$ and a radius of only 10 km! More information on neutron stars can be found in the review by Srinivasan (2002).

White dwarfs are found in many flavors. The most common spectral designations are DA, for those stars showing prominent hydrogen Balmer absorption features as in A type main-sequence stars, and DB, for those showing prominent helium (I) lines as in B type main-sequence stars. The "D" designates that the object is degenerate. Very hot white dwarfs (> 80,000 K) just beginning their evolution from the planetary nebula stage are labeled DO and show He (II) absorption lines. At the opposite regime of very cool temperatures (< 5,000 K), both hydrogen and helium lines are invisible in the spectra of white dwarfs; these featureless spectra are designated DC. Slightly hotter helium rich white dwarfs are also designated DC, as they also do not show any absorption lines.

Other designations include DQ white dwarfs (those with carbon lines), DH white dwarfs (magnetic white dwarfs) and DZ white dwarfs (those with other metal lines). Example spectra of each of these classes can be found in the first data release of the Sloan Digital Sky Survey (Kleinman et al. 2004).

The chemical evolution of white dwarfs is quite complicated and not completely understood (see e.g., Bergeron, Ruiz, & Leggett 1997). White dwarfs are believed to change spectral types, perhaps several times, through their evolution. The distribution of white dwarfs of various spectral classes as a function of temperature shows several gaps. For example, the DB gap, located at temperatures between 30,000 and 45,000 K, contains no DB white dwarfs. DB white dwarfs are, however, found both above and below the gap. At much cooler temperatures, between 5,000 and 6,000 K, a non-DA gap exists where only DA white dwarfs are present. Overall, the ratio of DA to non-DA white dwarfs is much greater (20:1) than at hot temperatures (~30,000 K). However, the DB and DC spectral type are abundant at cooler temperatures and the ratio drops to only 2:1 at temperatures under 10,000 K. It is believed that DA white dwarfs can have either thin ($10^{-10}M_\odot$) or thick ($10^{-4}M_\odot$) hydrogen surface layers. In the cases of thick surface layers, the stars will always remain of DA spectral type. However, for thin hydrogen layers, it is possible that the hydrogen layer mixes with the underlying more massive helium mantle ($10^{-2}M_\odot$) and is drowned out. This convective mixing requires cool temperatures and is a possible explanation for the abundance of cool non-DA white dwarfs. The non-DA gap may be explained by hydrogen accretion from the interstellar medium or from some yet unknown type of dilution or mixing of hydrogen and helium in that narrow temperature range.

More information on these issues as well as other parameters of white dwarfs can be found in the review paper by Fontaine, Brassard, & Bergeron (2001). Continued observations, such as those presented in this thesis, will help resolve these problems.

4. Interesting about white dwarfs

Over 99% of all stars will eventually end their lives as white dwarfs. These faint stellar remnants can be used in many different investigations. For example, white dwarfs cool with time in a predictable way. Recently, this white dwarf cooling process has been used to date the globular star cluster M4 (Hansen et al. 2004; Hansen et al. 2002) and independently determine the age of the Galactic halo. The same study also used white dwarfs to determine the mass function of the cluster above the main-sequence turn-off (Richer et al. 2004; Richer et al. 2002). Since all stars with a mass above 0.8 $M_\odot$ have evolved off the main-sequence in a 12 Gyr population, white dwarfs represent our only link to the distribution of stars (i.e., the initial mass function) of intermediate and massive stars in these systems. White dwarfs are also astrophysical important when considering the chemical evolution of the Galaxy. All stars with an initial mass up to 7 or 8 $M_\odot$ will end up becoming white dwarfs with a final mass less than 1.4 $M_\odot$. Therefore, many solar masses of material will be expelled into the interstellar medium during a star's evolution and therefore affect future nucleo-synthesis and star formation. A characterization of this mass loss, the initial-final mass relationship, remains today as one of the most poorly understood aspects of stellar evolution.

Recently, the possible nature of white dwarfs as Galactic dark matter candidates has been suggested by Alcock et al. (2000). Microlensing events towards the Large Magellanic Clouds suggest that approximately 20% of our Galactic halo is filled with 0.5 $M_\odot$ objects. A successful search for these objects by Oppenheimer et al. (2001) temporarily solved this long-standing problem. However, reanalysis of the results by several groups suggest that in fact Oppenheimer's population is not of halo origin and is more likely from a thick disk. Still, white dwarfs have not been excluded as a possible component of the Galactic dark matter.

Although white dwarfs are faint, studying them is becoming easier with larger telescopes and improved instrumentation. The few reasons listed above do not do justice to the number of interesting scientific developments that have resulted from studying white dwarfs. These studies range from using astro-seismology to probe the inner structure of these objects (see e.g., Kawaler1995, Fontaine & Brassard 1994), to improving models of white dwarf cooling and atmospheres (Hansen 1999; Bergeron, Saumon&Wesemael 1995; Wood 1995), to understanding the physics of matter at extreme densities, to using white dwarfs to determine the lower mass limit to type II supernovae (see e.g., Kaspi&Helfand 2002).

5. Summary of White Dwarfs in the Field

A 6-year baseline of imaging of the globular star cluster M4 has allowed us to separate out the cluster stars from the background spheroid population. Over this timescale, distant extragalactic sources have not moved and are identified using image morphology criteria. It is established a

zero-motion frame of reference using these galaxies and search for halo white dwarfs based on their morphology and kinematics. It was found that distinguishing faint galaxies from field stars is impossible when based solely on proper motions, and that an index of stellarity is crucial in separating the two classes. Based on the reduced proper motion diagram, it was identified nine thin/thick disk and three spheroid white dwarfs in these data. These numbers are consistent with the expected contribution of the conventional populations along the line of sight. Additionally, 2.5 dark halo white dwarfs are expected in these data based on a 20% white dwarf dark halo and are not found. The Poisson probability of getting zero events when 2.5 are expected is about 8%, and therefore our conclusion of not needing a dark halo population of white dwarfs to explain the present data is marginal. A similar study with the Advanced Camera for Surveys (ACS) on HST would be sensitive to many more potential dark halo white dwarfs and is desirable given the importance of this problem.

The extragalactic reference frame also allows us to perform two other important measurements. First, this fixed frame gives us an independent measurement of the fundamental Galactic constant, $\Omega_0 = \theta_0/R_0 = 25.3 \pm 2.4$ km/s/kpc. This provides a velocity of the Local Standard of Rest $v_{LSR} = \theta_0 = 203 \pm 23$ km/s at $R_0 = 8.0 \pm 0.5$ kpc, in agreement with independent studies. Secondly, the galaxies give us a direct measurement of M4's absolute proper motion, $\mu_\alpha = -12.26 \pm 0.47$ mas/yr, $\mu_\delta = -18.95 \pm 0.48$ mas/yr, also in good agreement with the latest studies.

6. Chandrasekhar limit and compact objects

In his investigations, Chandra incorporated special relativity in the analysis of white dwarfs, and found that the EDP is proportional to $\rho^{4/3}$ instead, demonstrating that the relativistic degeneracy pressure does not increase as rapidly as in Fowler's case. Performing an accurate study of the relativistic problem of a dense star ruled by a polytropic equation of state, in which gravity is countered by the EDP, he arrived at the celebrated Chandrasekhar mass limit [2]:

$$M_{Ch} = \frac{0.2}{(m_p \mu_e)^2} \left(\frac{\hbar c}{G}\right)^{3/2} \quad (1)$$

where $\hbar$, G, c, m_p and μ_e are the reduced Planck's constant, Newton's gravitational constant, speed of light, mass of a proton and mean molecular weight per electron, respectively. It is remarkable that such a significant result concerning stars should be expressible in terms of fundamental quantities (except for μ_e). In white dwarfs, the value of μ_e is about 2, so that from eq. (1) one finds the limit to be $M_{Ch} \approx 1.4 \, M_\odot$, where $M_\odot = 2 \times 1030$ kg is the Sun's mass.

The Chandrasekhar mass limit implies that no white dwarf with mass greater than this limit can hold out against gravitational collapse. So far, all the white dwarfs discovered (e.g. Sirius B, the companion star to Sirius) in the cosmos, have mass less than M_{Ch}. For masses beyond this limit, two prescient ideas were put forward independently, that played important roles later - one of Landau [6], before the discovery of neutrons by Chadwick in 1932 and the other by Baade and Zwicky [8,9], after the discovery. Landau had speculated that for stellar cores whose mass

exceeded M_{Ch}, the density would become so large due to shrinking that the atomic nuclei in the core would come in contact with each other – the whole core turning into a giant nucleus [6]. Baade and Zwicky, while attributing the origin of cosmic rays to stellar explosions called supernovae, correctly identified the energy liberated due to sudden decrease in the gravitational potential energy (as the core collapses rapidly to form a neutron star of radius ~10 km) as the one that powers supernova explosion [8,9].

7. Short Theoretical approach

Derivation of non-relativistic mass-radius relation

A. Review of the Macroscopic Calculation

By balancing the degeneracy pressure of the electrons in a white dwarf against the inward gravitational pressure from the nucleon mass, one can derive a semi-realistic formula for the radius of a white dwarf in terms of its mass, its nucleon-to-electron ratio, and fundamental constants. The simplest calculation assumes local charge neutrality and nonrelativistic electrons [1]. It is modeled the white dwarf as a uniform-density sphere of N nucleons and *fN*electrons confined to a radius R. Treating the electrons as a fermionic gas at zero temperature in a 3-dimensional infinite well, the outward degeneracy pressure is found to be

$$P_{deg} = \frac{2}{5}\frac{\hbar^2}{2m_e}\left(\frac{fN}{V}\right)^{5/3}(3\pi^2)^{2/3} \qquad (1)$$

where V is the volume of the star. The inward Newtonian gravitational pressure of the nucleons is given by

$$P_{grav} = -\frac{3}{5}G(Nm_p)^2\frac{(4\pi)^{1/3}}{(3V)^{4/3}} \qquad (2)$$

Balancing pressures and taking the mass M of the star to be Nm_p, we find the stable radius of the star to be

$$R \approx \frac{\hbar^2 f^{5/3}}{Gm_e m_p^{5/3}M^{1/3}} \qquad (3)$$

Note that the radius in Eq. 3 decreases as the star becomes heavier. Since the kinetic energy of the electron Fermi gas increases under adiabatic compression, the non-relativistic assumption breaks down for massive white dwarfs. In 1931, Chandrasekhar calculated the mass of a stable white dwarf with local charge neutrality using the equation of state for ultra-relativistic electrons,$P \propto \rho^{4/3}$. This lead to the surprising discovery of a maximum mass of $1.4M_\odot$ for stable white dwarfs, beyond which gravitational collapse occurs until the star is stabilized again by neutron degeneracy pressure [4].

B. The Fermi Surface Calculation of the White Dwarf Radius

Despite the elegance of the derivation leading to Eq. 3, it is somewhat unsatisfying that degeneracy pressure and gravitational pressure were treated separately. Here we present an alternative approach, in which the Fermi surface induced by a many-particle Hamiltonian including the gravitational potential leads to the radius of a white dwarf.

For simplicity, consider a white dwarf composed of N protons and N electrons. Assuming that the Coulomb force binds each electron to a single proton, in a first approximation the star can be considered a degenerate gas of N neutral spin -1/2 fermions with inertial mass me and gravitational mass mp. Note that since the kinetic energy is almost purely due to the electron, we need not consider the contribution from the spin -1/2 proton to the degeneracy pressure. In this model, the many-particle Hamiltonian of the neutral particles is

$$H = \sum_{i=1}^{N} \frac{p_i^2}{2m_e} - \sum_{1 < i < j \leq N} \frac{Gm_p^2}{r_{ij}} \quad (4)$$

which can be rewritten as

$$H = \sum_{i=1}^{N} \left[\sum_{j \neq i} \left(\frac{p_j^2}{2(N-1)m_e} - \frac{Gm_p^2}{2r_{ij}} \right) \right] \equiv \sum_{i=1}^{N} h_i \quad (5)$$

As pointed out by [1], hi represents the Hamiltonian of $N - 1$ non-interacting particles each with inertial mass $(N - 1)m_e$ and gravitational mass $m_p/2$ in the gravitational field of the ith particle, which is fixed and has gravitational mass m_p. The suggestive form of the h_i tempts us to calculate the ground state of h_i by filling the $N - 1$ lowest single-particle energy levels of a 1/r potential. Formally, the single-particle spectrum is identical to that of the hydrogen atom under the substitutions

$$e^2 \rightarrow G \left(\frac{1}{2} m_p \right) m_p \quad \text{and} \quad m_e \rightarrow (N - 1)m_e$$

$$\epsilon_n = - \frac{(N-1)(G^2 m_p^4 m_e)}{8\hbar^2 n^2} \quad (6)$$

where each ϵ_n has a degeneracy of $2n^2$. Thus,

$$N = \sum_{n=1}^{n_F} 2n^2 \approx \frac{2n_F^3}{3} \quad (7)$$

from which we can solve for the highest occupied level n_F. The total ground state energy in the gravitational field of the ith particle is then

$$E_i = \sum_{n=1}^{n_F} 2n^2 \epsilon_n \approx - \frac{N G^2 m_p^4 m_e n_F}{4\hbar^2} \approx - \left(\frac{3}{2} \right)^{1/3} \frac{N^{4/3} G^2 m_p^4 m_e}{4\hbar^2} \quad (8)$$

Furthermore, using the relation

$$\langle r_n \rangle \approx \frac{3}{2} n^2 a_0 \quad (9)$$

in the limit $n \gg \ell$, where a0 is the gravitational "Bohr radius" of the star, we see that the radius R and the mass $M \approx N/m_p$ of the white dwarf are related by

$$R = \langle r_n \rangle \approx 3 \left(\frac{3}{2} \right)^{2/3} \frac{2\hbar^2}{Gm_p^{5/3} m_e M^{1/3}} \quad (10)$$

which agrees with Eq. 3 up to a scaling factor. Strictly speaking, Eq. 10 only describes the radius of a zero-temperature fermionic gas under *one* of the h_i's in the sum in Eq. 5. If the h_i's were

independent, we could fill each h_i up to its Fermi level and find the total ground state energy to be NE_i. In reality, the h_i's share common coordinates and are not truly independent. [1] shows that, therefore, the ground state energy NE_i is a lower bound on the actual ground state energy.

Nonetheless, the microscopic derivation of the white dwarf ground state energy and radius motivates further investigation into the similarities between atoms and stars. We extend these techniques in the next section to estimate the effect of Coulomb forces on the ground state energy.

Accounting for Coulomb Interactions

A. Thomas-Fermi Theory

The Coulomb interaction is essential for keeping the electrons in a white dwarf close to the nuclei, thereby maintaining the local neutrality condition assumed above [1]. Although we could proceed with the approach from Section 2B and model the effective Coulomb interactions by adding another term to h_i, it soon becomes worthwhile to introduce a semiclassical approximation.

The basis of the Thomas-Fermi approximation is the postulate that electrons in a potential V(r) are uniformly distributed in phase space with two electrons per $(2\pi\hbar)^3$ of volume. This assumption is exactly true for free electrons; in a potential, the approximation is valid when the de Broglie wavelength of the particles is much shorter than the length scale over which the potential varies significantly. For every volume of coordinate space d3r, we define a local Fermi momentum $p_F(r)$ and a volume of occupied momentum space, $(4/3)\pi p^3_F(r)$, such that the total volume of occupied phase space in a sphere of radius R is $(4\pi/3)^2 R^3 p^3_F$. Equating the number of electrons in phase space to that in coordinate space, we find an expression for the local electron number density in terms of the local Fermi momentum:

$$n(r) = \frac{p_F^3(r)}{3\pi^2\hbar^3}(11)$$

Note that the r dependence in $p_F(r)$ arises from the spatial variation of the potential V (r).

Similarly, we define a local Fermi energy functional

$$E_F(n(r)) = \frac{p_F^2(r)}{2m_e} + V(r)(12)$$

E_F must be constant in coordinate space at equilibrium; otherwise, we could lower the ground state energy of the system by moving a particle from a region of higher E_F to one of lower E_F [1]. As an illustration of the Thomas-Fermi approximation, consider the total ground state energy functional for a white dwarf ignoring Coulomb contributions, given by the sum of kinetic and gravitational terms:

$$\vec{E}(n) = \overrightarrow{E_K}(n) + \overrightarrow{E_G}(n)(13)$$

where $\vec{E}(n)$ denotes a functional of n(r) and

$$\overrightarrow{E_G}(n) = -\frac{Gm_p^2}{2}\iint_0^R \frac{n(r)n(r`)}{|r-r`|}d^3rd^3r` \quad (14)$$

The kinetic energy functional in the ground state is obtained by integration in a volume of phase space $d^3r d^3p$ up to the local Fermi momentum [1]:

$$\vec{E}(n) = \int_0^R \int_0^{p_F} 2 \frac{d^3r d^3p}{8\pi^3\hbar^3} \frac{p^2}{2m_e} = \kappa \frac{\hbar^2}{m_e} \int_0^R n^{\frac{5}{3}}(r) d^3r \quad (15)$$

where $\kappa = (3\pi^2/10)(3/\pi)^{2/3}$ results from integrating over d^3p. Using Eq. 13, we can determine the number density and ground state energy by minimizing the density functional $\tilde{E}[n]$ over all $n(r)$. It is easily verified that doing so in the case of constant $n(r)$ and solving for the radius of minimum energy reproduces Eq. 3 up to a constant factor.

The Coulomb corrections

A. The non-relativistic Coulomb correction

In Section 2B, we considered the entire star as a single atom bound by gravity in order to study the gravitational effect on the ground state energy. Unlike gravity, electrostatic forces cancel out globally and therefore should be considered at atomic length scales. Up to this point, we have assumed all charges to be smeared out evenly in a neutral electron-nucleon fluid. We now collapse each nucleus into a point charge Ze surrounded by a uniform cloud of Z electrons. Each nucleus and its associated electrons are confined to a spherical cell of radius R_{cell}, and we ignore any Coulomb interactions between cells. Since realistic white dwarf stars have a characteristic density of $10^6 g/cm3$ and therefore are around 10^6 times denser than ordinary matter, R_{cell} is of order $10^{-2}a_0$, where a_0 is the Bohr radius [1].

1. With uniform electron density within cells

In a first calculation of the Coulomb correction, we take the electron number density within each cell to be the average of $n(r)$ over the cell volume, in which case the Thomas-Fermi approach is trivial. Calculating the Coulomb energy of a uniformly charged sphere interacting with a point nucleus, we find

$$E_{e-n}(R_{cell}) = -\frac{3}{2} \frac{Z^2 e^2}{R_{cell}} \quad (16)$$

while the electron-electron interaction energy is given by

$$E_{e-e}(R_{cell}) = \frac{3}{5} \frac{Z^2 e^2}{R_{cell}} \quad (17)$$

Thus, from a few simple calculations in basic electrostatics, we find that the first-order correction to the energy per cell is

$$E_C^{(1)}(cell) = -\frac{9}{10} \frac{Z^2 e^2}{R_{cell}} = -\frac{9}{10} \left(\frac{4\pi n_{avg}}{3}\right)^{1/3} Z^{5/3} e^2 \quad (18)$$

and the total first-order energy correction for the white dwarf is

$$E_C^{(1)} = -\frac{9}{10} \left(\frac{4\pi}{3}\right)^{1/3} \int_0^R n^{\frac{4}{3}}(r) d^3r \quad (19)$$

To estimate the size of the Coulomb correction, recall that the total kinetic energy is equal in magnitude to the total energy E[star] according to the Virial theorem.

Thus, we can consider the ratio of the Coulomb energy per cell to the kinetic energy per cell. From Eq. 15, the kinetic energy per cell at zeroth order in the Coulomb correction is

$$E_\kappa^{(0)}(cell) \approx \frac{\hbar^2}{m_e} n_{avg}^{\frac{5}{3}} R_{cell}^3 \approx e^2 \frac{a_0}{R_{cell}^2} Z^{\frac{5}{3}} \quad (20)$$

where a_0 is the usual Bohr radius. Thus,

$$\frac{E_C^{(1)}}{E(star)} \approx \frac{E_C^{(1)}(cell)}{E_\kappa^{(0)}(cell)} \approx \frac{R_{cell}}{a_0} Z^{1/3} \approx \frac{R}{a_0} \left(\frac{Z}{N}\right)^{1/3} \quad (21)$$

where N is the total number of cells. We see that for the Coulomb correction to be much less than the total energy, each cell must be compressed to a radius much less than the Bohr radius, which is in fact the case for white dwarfs [1].

2. A refined estimate of the electron density within each cell

We now apply the Thomas-Fermi approximation to show that in a self-consistent treatment of the Coulomb interactions, the electron density within each cell must be non-uniform. Our starting point is the electron Fermi energy functional E^F_e (Eq. 12) with the Coulomb potential given by $-V(r)/e$. (The gravitational contribution to V(r) has been absorbed by the parameter R_{cell}, which depends on the gravitational compression.) Note that $-V(r)/e$ must satisfy the Poisson equation

$$\nabla^2 V(r) = 4\pi e^2 \left(n_p(r) - n_e(r)\right) \quad (22)$$

For a single isolated cell with nuclear charge Ze, the potential would simply be $-Ze^2/r$. However, a lattice of net neutral, non-interacting cells such as a white dwarf is subject to the condition that the potential and its radial derivative vanish at the boundary of each cell. Thus, we define a dimensionless function $\phi(r)$ by

$$\frac{e^2 Z\phi(r)}{r} = E_e^F - V(r) \quad (23)$$

and a dimensionless coordinate

$$\eta = \frac{r}{b} \quad (24)$$

Where $b = (3\pi)^{2/3} \frac{\lambda_e}{\alpha} 2^{-7/3} Z^{-1/3}$ and λ_e is the electron Compton wavelength. The Poisson equation becomes

$$\frac{d^2\phi\eta}{d\eta^2} = \frac{\phi\eta^{3/2}}{\eta^{1/2}} \quad (25)$$

With $\phi(0) = 1$ for a point nucleus. The self-consistent electron distribution within the cell is given by [6].

$$n_e(\eta) = \frac{Z}{4\pi b^3} \left(\frac{\phi(\eta)}{\eta}\right)^{\frac{3}{2}} \quad (26)$$

Fig. 1 shows the electron density obtained by integrating Eq. 25 with appropriate boundary conditions. We see that the electron distribution is sharply peaked at the center of the cell and

quickly drops to zero, suggesting that the Coulomb energy is lower than in the uniform-density case. However, since regions of lower potential must have higher Fermi kinetic energy for the total Fermi energy to be spatially constant, relativistic effects become non-negligible near the center of the cell.
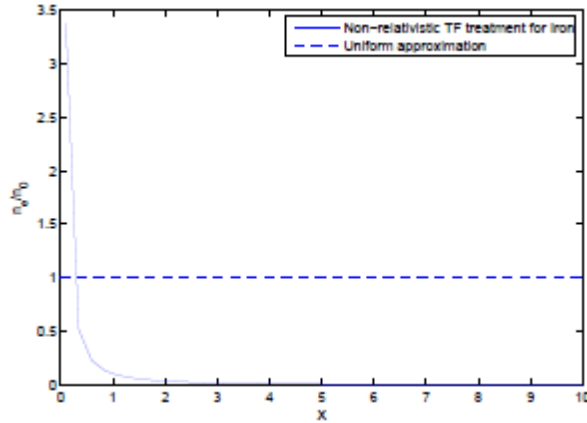

Figure 7.1: The electron number density n_e in units of the average electron number density n_0 within a cell as a function of the radial coordinate $x = r/\lambda_\pi$, where the pion Compton wavelength is used for comparison with Fig. 2. Results for cells with Iron nuclei were obtained by numerical integration of the non-relativistic TF equation 25.

B. The relativistic Coulomb correction

The non-relativistic treatment of the electrons breaks down for highly-compressed cells, as high electron kinetic energies are required to balance inward gravitational pressure. Feynman, Metropolis, and Teller [7] (FMT) have shown that the Thomas-Fermi model can be applied relativistically within cells to obtain the equation of state for compressed matter. Eq. 12 for the electron Fermi energy is replaced by the relativistic Fermi energy

$$E_e^F = \sqrt{c^2 (p_e^F)^2 + m_e^2 c^4} - m_e c^2 + V(r) \quad (27)$$

Unfortunately, the point-like nucleus approximation adopted in the previous section now leads us to a non-integrable expression for the electron density $n_e(r)$ at the origin, given by

$$n_e(r) = \frac{(p_e^F)^3}{3\pi^2 \hbar^3} = \frac{1}{3\pi^2 \hbar^3 c^3} \left(\dot{V}^2 + 2 m_e c^2 \dot{V} \right)^{3/2} \quad (28)$$

where $\dot{V} = E_e^F - V(r)$.

Following the approximation given in [6] for the nucleus size, we take the protons to be uniformly distributed up to a radius R_c in each cell, defined by

$$R_e = \Delta \lambda_\pi Z^{1/3} \quad (29)$$

Where $\lambda_\pi = \dfrac{\hbar}{m_\pi c}$ is the pion Compton wavelength and Δ is a factor proportional to the nuclear density that is is 1 for ordinary nuclei. The proton density is therefore

$$n_p(r) = \frac{Z}{\frac{4}{3}\pi R_e^3} \theta(r - R_e) = \frac{3}{4\pi (\Delta \lambda_\pi)^3} \theta(r - R_e) \quad (30)$$

Where θ is the Heaviside function.

As before, each cell is net neutral and there exist no electric fields between cells, so we impose the boundary conditions $V(R_{cell}) = 0$ and $dV/dr|_{r=Rcell} = 0$ on the solutions to the Poisson's equation for the potential 22.

Introducing the dimensionless variables $x = r/\lambda_\pi$, $x_c = R_c/\lambda_\pi$, $\chi/r = \dot{V}(r)/\hbar c$, we substitute the particle densities (30) and (28) into (22) to obtain the relativistic version of Eq. 25:

$$\frac{1}{3x}\frac{d^2\chi(x)}{dx^2} = -\frac{\alpha}{\Delta^3}\theta(x_e - x) + \frac{4\alpha}{9\pi}\left(\frac{\chi^2(r)}{x^2} + 2\frac{m_e}{m_\pi}\frac{\chi(x)}{x}\right)^{3/2} \quad (31)$$

Fig. 2 shows the electron distribution in a cell obtained by integrating the differential equation (31) with the appropriate boundary conditions. Rotondo et al. show in [5] that Eq. 31 leads to a maximum in the electron Fermi energy when $R_c = R_{cell}$. In contrast, the Fermi energy obtained from Eq. 25 grows without bound as $R_{cell} \to 0$ since the cell is infinitely compressible when the nucleus is a point charge.

8. Instability of compressed white dwarfs

We now review some results from the recent literature examining the behavior of white dwarfs in the limit of extremely high compression using the relativistic Thomas- Fermi equation.

At high mass densities and immense electron Fermi pressures, electrons and protons combine to form neutrons. This process, known as inverse beta decay, occurs
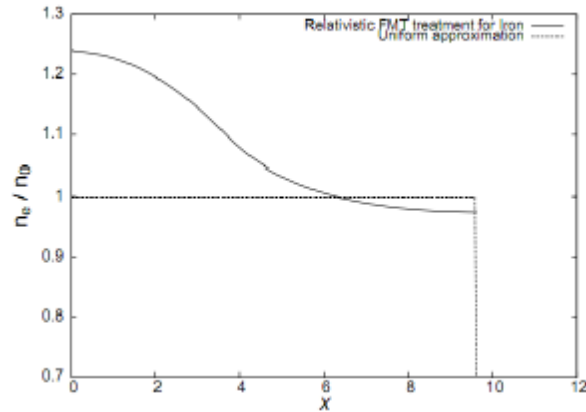

Figure8.1: The electron number density *ne* in units of the average electron number density *n0* within a cell as a function of the radial coordinate x/λ_π, obtained by numerical integration of the relativistic FMT equation. Results for cells composed of Iron nuclei are shown. Adapted from [6].
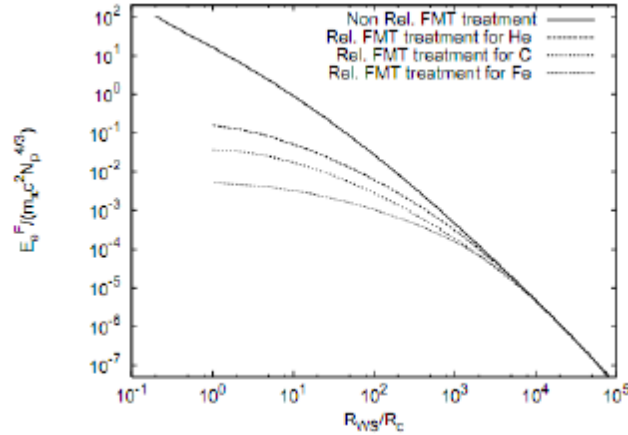
Figure 8.2: The electron Fermi energies with a cell as a function of the cell radius using the nonrelativistic and relativistic differential equations. R corresponds to R_{cell} and N_p to Z in our notation. The results agree at large radii (low compression) but the non-relativistic energy diverges as $R \to 0$. Adapted from [5].

when the kinetic energy of the electons exceeds the massenergy difference between a nucleus (Z, A) and a nucleus (Z-1, A). Empirical values of the critical inverse beta decay energy ϵ_{crit} for ^{4}He and ^{56}Fe are around 20.6 MeV and 3.7 MeV, respectively [6]. In the uniform density approximation for the electron fluid, the critical density is given by

$$\rho_{crit}^{unif} = \frac{Z}{A} \frac{m_p}{3\pi^2 \hbar^3 c^3} \left((\epsilon_{crit})^2 + 2m_e c^2 \epsilon_{crit} \right)^{3/2} (1)$$

Using $\rho = (A/Z)m_N n_e$ with n_e in terms of the relativistic Fermi momentum. The values for ^{4}He and ^{56}Fe are around 1.37×10^{11} and 1.14×10^9 g cm^{-3}, respectively.

Improving upon the uniform-density estimate, Rueda et. al [6] found numerical solutions for the electron density from Eq. 31 subject to the equilibrium condition $\mu_n = \mu_e + \mu_p$, where μ is the chemical potential of each species. As the chemical potential is proportional to the Fermi energy, the equilibrium condition is

$$E_n^F = \sqrt{c^2 (p_n^F)^2 + m_n^2 c^4} - m_n c^2 = \sqrt{c^2 \left(p_p^F\right)^2 + m_p^2 c^4} - m_p c^2 - V(r) + E_e^F (2)$$

Where $p_n^F(n_n(r))$ is determined by Eq. 11 and $V(r)$ is negative because of the positive charge of the proton.

This condition determines the neutron density $n_n(r)$. For each mass number A, there also exists a numerical relation between the number of protons per nucleus Z and the electron Fermi energy $E^F{}_e$. Since the density of the star is determined by $E^F{}_e$, A, and Z, numerical values of the critical density for inverse beta decay can be obtained using this method. Rueda et al. [6] found values of

1.2×10^{12} and 8.6×10^{8} g cm^{-3} for ^{4}He and ^{56}Fe, which is greater for the lighter nuclei and less for the heavier nuclei than in the uniform approximation.

As a final remark, we mention that general relativistic corrections to the equations of state for a white dwarf emerge as another source of instability at high densities. While we regret that the Tolman-Oppenheimer- Volkov (TOV) equations of equilibrium for general relativistic matter are beyond the scope of this discussion, it is worthwhile to mention that we can derive a post-Newtonian equation satisfied by the chemical potential within a cell by expanding the TOV equations to first order in the ratio of pressure to energy density of the cell and $GM/(c^{2}r)$. Numerical solutions to the post- Newtonian equations show that in addition to the critical mass imposed by beta decay stability, a white dwarf has a critical mass due to the general relativistic corrections.

Interestingly, Rueda et al. [6] have found that the onset of general relativistic instability for ^{4}He white dwarfs occurs at lower densities than for beta decay instability, whereas the behavior of ^{56}Fe white dwarfs is the opposite. Thus, using TF theory, we see that the instability of stars of light material is due to general relativistic effects while that of heavy material is due to inverse beta decay.

9. Observations

What should be mentioned here is that important studies were made upon the Gemini constellation and the NGC 2099 cluster. We leave here some references for more detailed studies of white dwarfs and the information that can be obtained from these studies. As a starting point, it can be found in J.S. Kalirai, Astrophisics in White Dwarfs (2004), Kalirai et al. 2001c and Murowinski, R. et al. 2002.

V.   Neutron Stars

1. Magnetars

Neutron stars-such as Magnetar are the densest material objects known, packing slightly more than the sun's mass inside a ball just 20 kilometers across. Based on the study of SGRs, it seems that some neutron stars have magnetic fields so intense that they radically alter the material within them and the state of the quantum vacuum surrounding them, leading to physical effects observed nowhere else in the universe.

Because The MARCH 1979 Burst was so bright, theorists at the time reckoned that its source was in our galactic neighborhood, hundreds of light-years from Earth at most. If that had been true, the intensity of the x-rays and gamma rays would have been just below the theoretical maximum steady luminosity that can be emitted by a star. That maximum, first derived in 1926 by English astrophysicist Arthur Eddington, is set by the force of radiation flowing through the hot outer layers of a star. If the radiation is any more intense, it will overpower gravity, blow away ionized matter and destabilize the star. Emission below the Eddington limit would have been fairly straightforward to explain. For example, various theorists proposed that the outburst was triggered by the impact of a chunk of matter, such as an asteroid or a comet, onto a nearby neutron star. But observations soon confounded that hypothesis. Each spacecraft had recorded the time of arrival of the hard initial pulse.

These data allowed astronomers, led by Thomas Lytton Cline of the NASA Goddard Space Flight Center, to triangulate the burst source. The researchers found that the position coincided with the Large Magellanic Cloud, a small galaxy about 170,000 light-years away. More specifically, the event's position matched that of a young supernova remnant, the glowing remains of a star that exploded 5,000 years ago. Unless this overlap was pure coincidence, it put the source 1,000 times as far away as theorists had thought and thus made it a milliontimes brighter than the Eddington limit. In 0.2 second the March 1979 event released as much energy as the sun radiates in roughly 10,000 years, and it concentrated that energy in gamma rays rather than spreading it across the electromagnetic spectrum. No ordinary star could account for such energy, so the source was almost certainly something out of the ordinary either a black hole or a neutron star. The former was ruled out by the eight-second modulation: a black hole is a featureless object lacking the structure needed to produce regular pulses. The association with the supernova remnant further strengthened the case for a neutron star. Neutron stars are widely believed to form when the core of a massive but otherwise ordinary star exhausts its nuclear fuel and abruptly collapses under its ownweight, thereby triggering a supernova explosion.Identifying the source as a neutron star did not solve the puzzle;on the contrary, it merely heightened the mystery. Astronomers knew several examples of neutron stars that lie within supernova remnants. These stars were radio pulsars, objects that are observed to blink on and off in radio

waves. Yet the March 1979 burster, with an apparent rotation period of eight seconds, was spinning much more slowly than any radio pulsar then known. Even when not bursting, the object emitted a steady glow of x-rays with more radiant power than could be supplied by the rotation of a neutron star. Oddly, the star was significantly displaced from the center of the supernova remnant. If it was born at the center, as is likely, then it must have recoiled with a velocity of about 1,000 kilometers per second at birth.Such high speed was considered unusual for a neutron star. Finally, the outbursts themselves seemed inexplicable. X-ray flashes had previously been detected from some neutron stars, but they never exceeded the Eddington limit by very much. Astronomers ascribed them to thermonuclear fusion of hydrogen or helium or to the sudden accretion of matter onto the star. But the brightness of the SGR bursts was unprecedented, so a new physical mechanism seemed to be required.

Spin Forever Down

The final burst from the March 1979 source was detected in May 1983; none has been seen in the 19 years since. Two other SGRs, both within our Milky Way galaxy, went off in 1979 and have remained active, emitting hundreds of bursts in the years since. A fourth SGR was located in 1998. Three of these four objects have possible, but unproved, associations with young supernova remnants. Two also lie near very dense clusters of massive young stars, intimating that SGRs tend to from such stars. A fifth candidate SGR has gone off only twice;its precise location is still unknown.As Los Alamos National Laboratory scientists Baolian L.Cheng, Richard I. Epstein, Robert A. Guyer and C. Alex Young pointed out in 1996, SGR bursts are statistically similar to earthquakes.The energies have very similar mathematical distributions,with less energetic events being more common. Our graduate student Ersin Gögüs of the University of Alabama at Huntsville verified this behavior for a large sample of bursts from various sources. This and other statistical properties are a hallmark of self-organized criticality, whereby a composite system attains a critical state in which a small perturbation can trigger a chain reaction. Such behavior occurs in systems as diverse as avalanches on sandpiles and magnetic flares on the sun.But why would a neutron star behave like this? The solution emerged from an entirely separate line of work, on radio pulsars. Pulsars are widely thought to be rapidly rotating, magnetized neutron stars. The magnetic field, which is supported by electric currents flowing deep inside the star, rotates with the star. Beams of radio waves shine outward from the star's magnetic poles and sweep through space as it rotates, like lighthouse beacons—hence the observed pulsing. The pulsar also blows out a wind of charged particles and low-frequency electromagnetic waves, which carry away energy and angular momentum, causing its rate of spin to decrease gradually. Perhaps the most famous pulsar lies within the Crab Nebula, the remnant of a supernova explosion that was observed in 1054. The pulsar rotates once every 33 milliseconds and is currently slowing at a rate of about 1.3 millisecond every century. Extrapolating backward, it was born rotating once every 20 milliseconds. Astronomers expect it to continue to spin down,eventually reaching a point when its rotation will be too slow to power

the radio pulses. The spin-down rate has been measured for almost every radio pulsar, and theory indicates that it depends on the strength of the star's magnetic field. From this, most young radio pulsars are inferred to have magnetic fields between 1012 and 1013 gauss. For comparison, a refrigerator magnet has a strength of about 100 gauss.
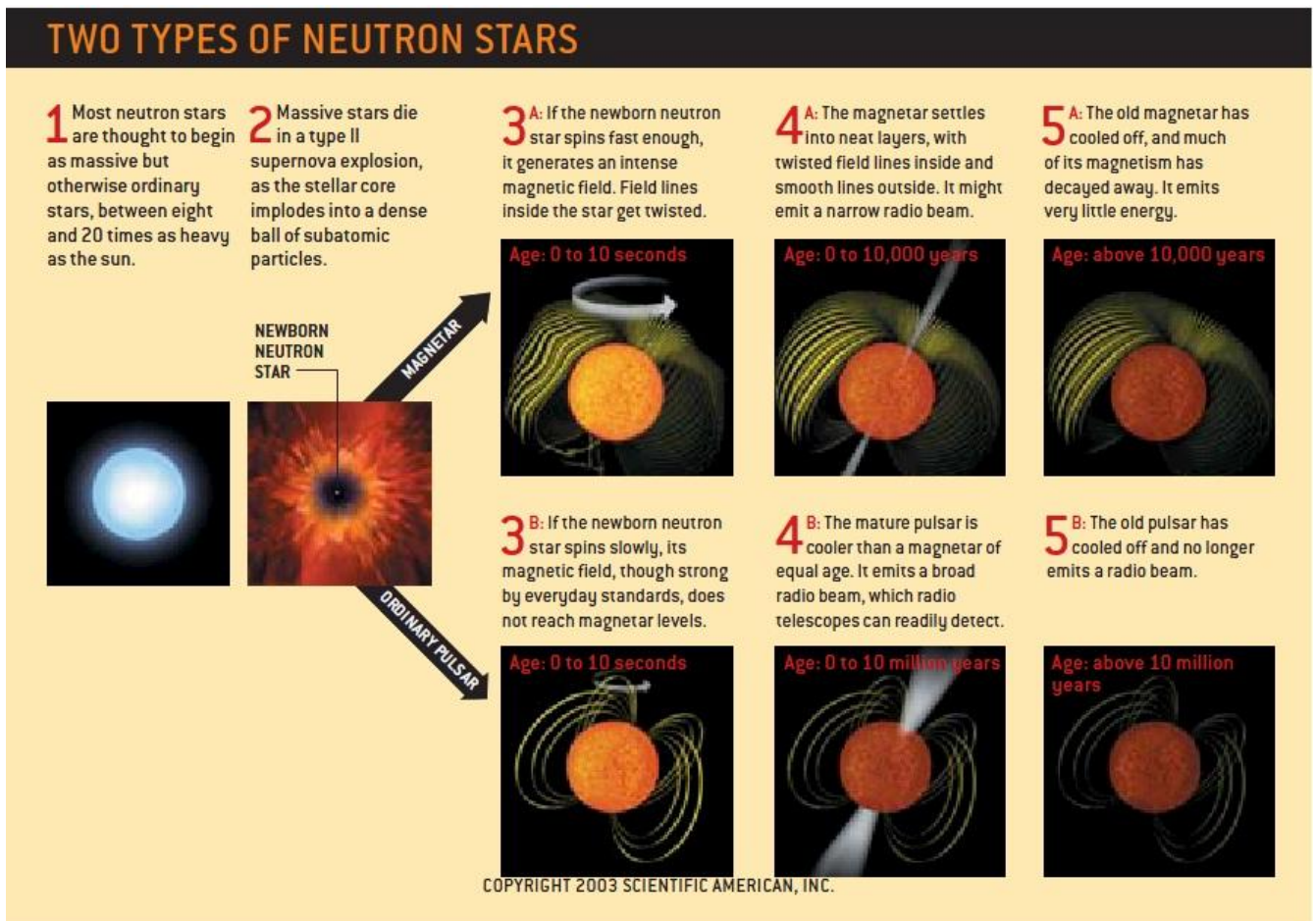
The Ultimate Convection Oven

Where did the magnetic field come from in the first place? The traditional assumption was: it is as it is, because it was as it was. That is, most astronomers supposed that the magnetic field is a relic of the time before the star went supernova. All stars have weak magnetic fields, and those fields can be amplified simply by the act of compression. According to Maxwell's equations of electromagnetism, as a magnetized object shrinks by a factor of two, its magnetic field strengthens by a factor of four. The core of a massive star collapses by a factor of 105 from its birth through neutron star formation, so its magnetic field should become 1010 times stronger.
If the core magnetic field started with sufficient strength, this compression could explain pulsar magnetism. Unfortunately, the magnetic field deep inside a star cannot be measured, so this simple hypothesis cannot be tested. There are also good reasons to believe that compression is only part of the story. Within a star, gas can circulate by convection. Warm parcels of ionized gas rise, and cold ones sink. Because ionized gas conducts electricity well, any magnetic field lines threading the gas are dragged with it as it moves. The field can thus be reworked and sometimes amplified. This phenomenon, known as dynamo action, is thought to generate the magnetic fields of stars and planets. A dynamo might operate during each phase of the life of a massive star, as long as the turbulent core is rotating rapidly enough. Moreover, during a brief period after the core of the star turns into a neutron star, convection is especially violent. This was first shown in computer simulations in 1986 by Adam Burrows of the University of Arizona and James M. Lattimer of the State University of New York at Stony Brook. They found that temperatures in a newborn neutron star exceed 30 billion kelvins. Hot nuclear fluid circulates in 10 milliseconds or less, carrying enormous kinetic energy. After about 10 seconds, the convection ceases.

Not long after Burrows and Lattimer conducted their first simulations, Duncan and Thompson, then at Princeton University,estimated what this furious convection means for neutronstar magnetism. The sun, which undergoes a sedate version of the same process, can be used as a reference point. As solar fluid circulates, it drags along magnetic field lines and gives up about 10 percent of its kinetic energy to the field. If the moving fluid in a newborn neutron star also transfers a tenth of its kinetic energy to the magnetic field, then the field would grow stronger than 1015 gauss, which is more than 1,000 times as strong as the fields of most radio pulsars.Whether the dynamo operates globally (rather than in limited regions) would depend on whether the star's rate of rotation was comparable to its rate of convection. Deep inside the sun, these two rates are similar, and the magnetic field is able to organize itself on large scales. By

analogy, a neutron star born rotating as fast as or faster than the convective period of 10 milliseconds could develop a widespread, ultrastrong magnetic field. In 1992 we named these hypothetical neutron stars "magnetars."An upper limit to neutron-star magnetism is about 1017 gauss; beyond this limit, the fluid inside the star would tend to mix and the field would dissipate. No known objects in the universe can generate and maintain fields stronger than this level.

One ramification of our calculations is that radio pulsars are neutron stars in which the large-scale dynamo has failed to operate.

In the case of the Crab pulsar, the newborn neutron star rotated once every 20 milliseconds, much slower than the rate of convection, so the dynamo never got going.

TWO TYPES OF NEUTRON STARS

1 Most neutron stars are thought to begin as massive but otherwise ordinary stars, between eight and 20 times as heavy as the sun.

2 Massive stars die in a type II supernova explosion, as the stellar core implodes into a dense ball of subatomic particles.

NEWBORN NEUTRON STAR

MAGNETAR

ORDINARY PULSAR

3 A: If the newborn neutron star spins fast enough, it generates an intense magnetic field. Field lines inside the star get twisted.

Age: 0 to 10 seconds

4 A: The magnetar settles into neat layers, with twisted field lines inside and smooth lines outside. It might emit a narrow radio beam.

Age: 0 to 10,000 years

5 A: The old magnetar has cooled off, and much of its magnetism has decayed away. It emits very little energy.

Age: above 10,000 years

3 B: If the newborn neutron star spins slowly, its magnetic field, though strong by everyday standards, does not reach magnetar levels.

Age: 0 to 10 seconds

4 B: The mature pulsar is cooler than a magnetar of equal age. It emits a broad radio beam, which radio telescopes can readily detect.

Age: 0 to 10 million years

5 B: The old pulsar has cooled off and no longer emits a radio beam.

Age: above 10 million years

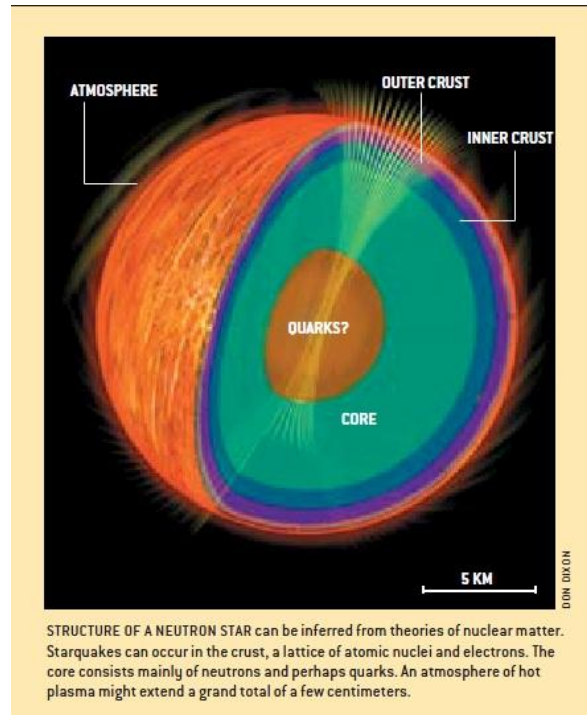COPYRIGHT 2003 SCIENTIFIC AMERICAN, INC.

Crinkle Twinkle Little Magnetar

Although we did not develop the magnetar concept to explain SGRs, its implications soon became apparent to us. The magnetic field should act as a strong brake on a magnetar's rotation. Within 5,000 years a field of 1015 gauss would slow the spin rate to once every eight seconds—neatly explaining the oscillations observed during the March 1979 outburst. As the field evolves, it changes shape, driving electric currents along the field lines outside the star. These currents, in

turn, generate x-rays. Meanwhile, as the magnetic field moves through the solid crust of a magnetar, it bends and stretches the crust.This process heats the interior of the star and occasionally breaks the crust in a powerful "starquake." The accompanying release of magnetic energy creates a dense cloud of electrons and positrons, as well as a sudden burst of soft gamma rays—accounting for the fainter bursts that give SGRs their name.

More infrequently, the magnetic field becomes unstable and undergoes a large-scale rearrangement. Similar (but smaller) upheavals sometimes happen on the sun, leading to solar flares. A magnetar easily has enough energy to power a giant flare such as the March 1979 event. Theory indicates that the first half-second of that tremendous outburst came from an expanding fireball. In 1995 we suggested that part of the fireball was trapped by the magnetic field lines and held close to the star. This trapped fireball gradually shrank and then evaporated, emitting x-rays all the while. Based on the amount of energy released, we calculated the strength of the magnetic field needed to confine the enormous fireball pressure: greater than 1014 gauss, which agrees with the field strength inferred from the spin-down rate. A separate estimate of the field had been given in 1992 by Bohdan Paczyn´ski of Princeton. He noted that x-rays can slip through a cloud of electrons more easily if the charged particles are immersed in a very intense magnetic field. For the x-rays during the burst to have been so bright, the magnetic field must have been stronger than 1014 gauss. What makes the theory so tricky is that the fields are stronger than the quantum electrodynamic threshold of 4×1013 gauss. In such strong fields, bizarre things happen. X-ray photons readily split in two or merge together. The vacuum itself is polarized, becoming strongly birefringent, like a calcite crystal. Atoms are deformed into long cylinders thinner than the quantum-relativistic wavelength of an electron [see box on opposite page]. All these strange phenomena have observable effects on magnetars. Because this physics was so exotic, the theory attracted few researchers at the time.

STRUCTURE OF A NEUTRON STAR can be inferred from theories of nuclear matter. Starquakes can occur in the crust, a lattice of atomic nuclei and electrons. The core consists mainly of neutrons and perhaps quarks. An atmosphere of hot plasma might extend a grand total of a few centimeters.

Zapped Again

As these THEORETICAL developments were slowly unfolding, observers were still struggling to see the objects that were the sources of the bursts. The first opportunity came when NASA's orbiting Compton Gamma Ray Observatory recorded a burst of gamma rays late one evening in October 1993. This was the break Kouveliotou had been looking for when she joined the Compton team in Huntsville. The instrument that registered the burst could determine its position only to within a fairly broad swath of sky. Kouveliotou turned for help to the Japanese ASCA satellite. Toshio Murakami of the Institute of Space and Astronautical Science in Japan and his collaborators soon found an x-ray source from the same swath of sky. The source held steady, then gave off another burst—proving beyond all doubt that it was an SGR. The same object had first been seen in 1979 and, based on its approximate celestial coordinates, was identified as SGR 1806–20. Now its position was fixed much more precisely, and it could be monitored across the electromagnetic spectrum. The next leap forward came in 1995, when NASA launched the Rossi X-ray Timing Explorer (RXTE), a satellite designed to be highly sensitive to variations in x-ray intensity. Using this instrument, Kouveliotou found that the emission from SGR1806–20 was oscillating with a period of 7.47 seconds—amazingly close to the 8.0-second periodicity observed in the March 1979 burst (from SGR 0526–66). Over the course of five years, the SGR slowed by nearly two parts in 1,000. Although the slowdown may seem small, it is faster than that of any radio pulsar known, and it implies a magnetic field approaching 1015 gauss. More thorough tests of the magnetar model would require a second giant flare. Luckily, the heavens soon complied. In the early morning of August 27, 1998, some 19 years after the

giant flare that began SGR astronomy was observed, an even more intense wave of gamma rays and x-rays reached Earth from the depths of space. It drove detectors on seven scientific spacecraft to their maximum or off scale. One interplanetary probe, NASA's Comet Rendezvous Asteroid Flyby, was forced into a protective shutdown mode. The gamma rays hit Earth on its nightside, with the source in the zenith over the mid-Pacific Ocean. Fortuitously, in those early morning hours electrical engineer Umran S. Inan and his colleagues from Stanford University were gathering data on the propagation of very low frequency radio waves around Earth. At 3:22 A.M. PDT, they noticed an abrupt change in the ionized upper atmosphere. The inner edge of the ionosphere plunged down from 85 to 60 kilometers for five minutes. It was astonishing. This effect on our planet was caused by a neutron star far across the galaxy, 20,000 light-years away.

Another Magneto Marvel

The August 27 FLARE was almost a carbon copy of the March 1979 event. Intrinsically, it was only one tenth as powerful, but because the source was closer to Earth it remains the most intense burst of gamma rays from beyond our solar system ever detected. The last few hundred seconds of the flare showed conspicuous pulsations, with a 5.16-second period. Kouveliotou and her team measured the spin-down rate of the star with RXTE; sure enough, it was slowing down at a rate comparable to that of SGR 1806–20, implying a similarly strong magnetic field. Another SGR was placed into the magnetar hall of fame.

HOW MAGNETAR BURSTS HAPPEN
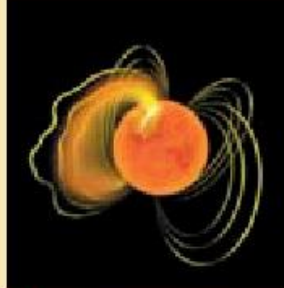
THE MAGNETIC FIELD OF THE STAR is so strong that the rigid crust sometimes breaks and crumbles, releasing a huge surge of energy.

1 Most of the time the magnetar is quiet. But magnetic stresses are slowly building up.

2 At some point the solid crust is stressed beyond its limit. It fractures, probably into many small pieces.

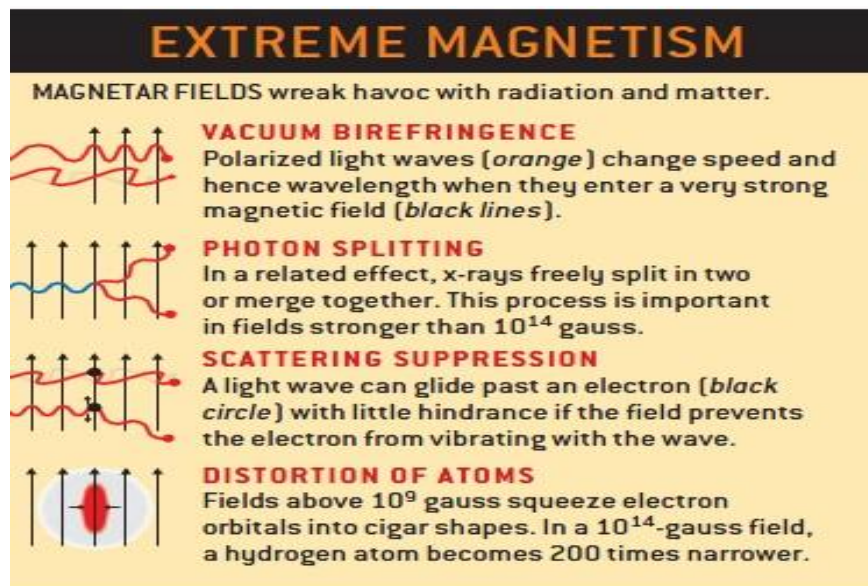3 This "starquake" creates a surging electric current, which decays and leaves behind a hot fireball.

4 The fireball cools by releasing x-rays from its surface. It evaporates in minutes or less.

The precise localizations of SGRs in x-rays have allowed them to be studied using radio and infrared telescopes (though not in visible light, which is blocked by interstellar dust). This work has been pioneered by many astronomers, notably Dale Frail of the National Radio Astronomy Observatory and Shri Kulkarni of the California Institute of Technology. Other observations have shown that all four confirmed SGRs continue to release energy, albeit faintly, even between

outbursts. "Faintly" is a relative term: this x-ray glow represents 10 to 100 times as much power as the sun radiates in visible light.

By now one can say that magnetar magnetic fields are better measured than pulsar magnetic fields. In isolated pulsars, almost the only evidence for magnetic fields as strong as 1012 gauss comes from their measured spin-down. In contrast, the combination of rapid spin-down and bright x-ray flares provides several independent arguments for 1014- to 1015-gauss fields in magnetars. As this article goes to press, Alaa Ibrahim of the NASA Goddard Space Flight Center and his collaborators have reported yet another line of evidence for strong magnetic fields in magnetars: x-ray spectral lines that seem to be generated by protons gyrating in a 10-15-gauss field. One intriguing question is whether magnetars are related to cosmic phenomena besides SGRs. The shortest-duration gamma-ray bursts, for example, have yet to be convincingly explained, and at least a handful of them could be flares from magnetars in other galaxies. If seen from a great distance, even a giant flare would be near the limit of telescope sensitivity.

EXTREME MAGNETISM

MAGNETAR FIELDS wreak havoc with radiation and matter.

VACUUM BIREFRINGENCE
Polarized light waves (*orange*) change speed and hence wavelength when they enter a very strong magnetic field (*black lines*).

PHOTON SPLITTING
In a related effect, x-rays freely split in two or merge together. This process is important in fields stronger than 10^{14} gauss.

SCATTERING SUPPRESSION
A light wave can glide past an electron (*black circle*) with little hindrance if the field prevents the electron from vibrating with the wave.

DISTORTION OF ATOMS
Fields above 10^9 gauss squeeze electron orbitals into cigar shapes. In a 10^{14}-gauss field, a hydrogen atom becomes 200 times narrower.

Only the brief, hard, intense pulse of gamma rays at the onset of the flare would be detected, so telescopes would register it as a GRB. Thompson and Duncan suggested in the mid-1990s that magnetars might also explain anomalous x-ray pulsars, a class of objects that resemble SGRs in many ways. The one difficulty with this idea was that AXPs had not been observed to burst. Recently, however, Victoria M. Kaspi and Fotis P. Gavriil of McGill University and Peter M. Woods of the National Space and Technology Center in Huntsville detected bursts from two of the seven known AXPs. One of these objects is associated with a young supernova remnant in the constellation Cassiopeia. Another AXP in Cassiopeia is the first magnetar candidate to have been detected in visible light. Ferdi Hulleman and Marten van Kerkwijk of Utrecht University in the Netherlands,working with Kulkarni, spotted it three years ago, and Brian Kern and

Christopher Martin of Caltech have since monitored its brightness in visible light. Though exceedingly faint, the AXP fades in and out with the x-ray period of the neutron star. These observations lend support to the idea that it is indeed a magnetar. The main alternative—that AXPs are ordinary neutron stars surrounded by disks of matter—predicts too much visible and infrared emission with too little pulsation. In view of these recent discoveries, and the apparent silence of the Large Magellanic Cloud burster for nearly 20 years, it appears that magnetars can change their clothes. They can remain quiescent for years, even decades, before undergoing sudden periods of extreme activity.

Some astronomers argue that AXPs are younger on average than SGRs, but this is still a matter of debate. If both SGRs and AXPs are magnetars, then magnetars plausibly constitute a substantial fraction of all neutron stars. The story of magnetars is a sobering reminder of how much we have yet to understand about our universe. Thus far, we have discerned at most a dozen magnetars among the countless stars. They reveal themselves for a split second, in light that only the most sophisticated telescopes can detect. Within 10,000 years, their magnetic fields freeze and they stop emitting bright x-rays. So those dozen magnetars betray the presence of more than a million, and perhaps as many as 100 million, other objects old magnetars that long ago went dark. Dim and dead, these strange worlds wander through interstellar space. What other phenomena, so rare and fleeting that we have not recognized them, lurk out there?

2. Neutron Stars as Quantum Systems

A neutron star is about 20 km in diameter and has the mass of about 1.4 times that of our Sun. This means that a neutron star is so dense that on Earth, one teaspoonful would weigh a billion tons! Because of its small size and high density, a neutron star possesses a surface gravitational field about 2×10^{11} times that of Earth. Neutron stars can also have magnetic fields a million times stronger than the strongest magnetic fields produced on Earth.

Neutron stars are one of the possible ends for a star. They result from massive stars which have mass greater than 4 to 8 times that of our Sun. After these stars have finished burning their nuclear fuel, they undergo a supernova explosion. This explosion blows off the outer layers of a star into a beautiful supernova remnant. The central region of the star collapses under gravity. It collapses so much that protons and electrons combine to form neutrons. Hence the name "neutron star".

Neutron stars may appear in supernova remnants, as isolated objects, or in binary systems. Four known neutron stars are thought to have planets. When a neutron star is in a binary system, astronomers are able to measure its mass. From a number of such binaries seen with radio or X-ray telescopes, neutron star masses has been found to be about 1.4 times the mass of the Sun. For binary systems containing an unknown object, this information helps distinguish whether the

object is a neutron star or a black hole, since black holes are more massive than neutron stars. Blackholesand neutronstars aresomeofthe most interestingobjects inthe universe because they are large enough to have significant gravitationa linfluence, yet compact enough to be described by the laws of quantum mechanics. It is well known that a neutron star is supported against its own gravity by exclusion-principle repulsion. Therefore, it can be reasoned that a neutron star can be described as a quantum system, such as an atom, in which each neuron is found in its own energy level.

"Would this model actually work in describing a neutron star?"
These calculations demonstrate the true liberating power of mathematics and science. Because the same laws hold everywhere throughout the universe, one ca nuse these basic equations to describe nearly everything-even neutron stars. It is the consistency, predictability, power and elegance o fthese laws that makes science so attractive.

First, it is assumed that the neutron star can be described by the "old"quantum mechanics, specifically the Schrodinger Equation, and that Newtonian gravity provides a good approximation of the gravitational field in the neutron star. Second, that the density of the neutron star is uniform. From this, one can work out the potential energy of each neutron star. The gravitational field at a point distance r from the center is given by $g = GMr/R^3$. Thus the gravitational potential (relative to the center) is given by:

$$V(r) = \frac{GM\,m_n}{2R^3}r^2 \equiv \frac{1}{2}kr^2 \quad (1)$$

the potential for a harmonic oscillator.The solutions to this problemare of the form $\Psi = F_i(x)F_j(y)F_k(z)$, where $F_n(x)$ is the nth solution toa1-dimensional harmonic oscillator. The total energy of this system is $(\hbar\omega\frac{1}{2} + i + j + k)$, where $\omega = \sqrt{k/m_n}$. Thus, the total energy only depends on the quantity $i + j + k$, which we denote as n. There are $\frac{1}{2}n(n-1)$degenerate orbital for each value of n, meaning that $n(n-1) \approx n^2$neutrons can reside in each "shell".

If one calculates the density at any point from the wavefunction, the density would be fairly uniform. But because they would not fit into this rectangle, it is better to exclude them. The density could be described as

$$\rho \sim (1 + 2(\tfrac{r}{R})^2)\sqrt{(1 - (\tfrac{r}{R})^2} \quad (2)$$
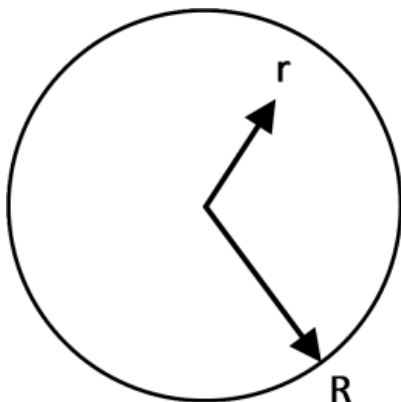
Which   is
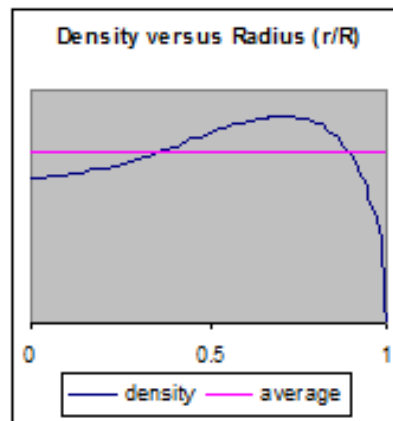
certainly not constant, but as the graph shows, does not deviate too drastically either. What is most interesting about this model is that it can predict the size of the neutron star. We know that, since n^2 neutrons reside in the nth shell, then a neutro nstar with n filled shells has $2n^3$ neutrons. If there are N neutrons in the star, then then value for the outermost filled shell is:

$$n = 3\sqrt{\frac{3}{2}N} = 3\sqrt{\frac{3M}{2m_n}} \qquad (3)$$

and its energy is very nearly $3M/2m_n$. Now we equate the "classical"energy $V(R)$ with the quantum energy and get:

$$\frac{GMm_n}{2R^3}R^2 = \frac{1}{2}kR^2 = \hbar\omega n = \hbar\sqrt{\frac{GMm_n}{R^3m_n}} \times 3\sqrt{\frac{3M}{2m_n}} \qquad (4)$$

This is an equation containing only R,M and several fundamental constants.Solving for R,one can find

$$R = 2 \cdot 3^{1/3}\frac{\hbar^2}{Gm_n{}^{8/3}}M^{-1/3} \qquad (5)$$

Which looks atrocious to most people, but gives some important insight: The size of a neutron star decreases as a mass increases. This is what my astronomy teacher said. Also note that it is fairly accurate. For a 2.0 solar mass neutron star, i tpredicts a radius of 7.8 km.

Of course, the neutron star can only get so small, and when its radius equals its Schwarzschild Radius, it must become a blackhole. This equation is even nastier:

$$\frac{2GM}{c^2} = 2 \cdot 3^{1/3}\frac{\hbar^2}{Gm_n{}^{8/3}}M^{-1/3} \qquad (6)$$

Which becomes

$$M = 2^{3/4}3^{1/4}(\frac{\hbar c}{G})^{3/4}\frac{1}{m_n^2} \qquad (7)$$

This threshold mass is 1.07×10^{31}kg,or about 5.64 solar masses. This limit is believed to be between 3 and 5 solar masses, so this estimate is not very far off, especially considering the crude assumptions used.

3. Exploring neutron stars (dense baryonic matter) in the laboratory

The understanding of aggregates of matter in terms of its elementary constituents and their interactions is a problem of fundamental interest with far reaching ramifications in science and technology. The only way to compress nuclear matter in a laboratory is to accelerate heavy atomic nuclei at high energy and to collide them.

Why study compressed baryonic matter, or more generally strongly interacting matter at high densities and temperature? Most obviously, because it's an important piece of Nature. The whole universe, in the early moments of the big bang, was filled with the stuff. Today, highly compressed baryonic matter occurs in neutron stars and during crucial moments in the development of supernova. Compressed baryonic matter is a material we can produce in the novel, challenging experiments that probe new experiments of temperature and density. On the theoretical side , it is a mathematically well-defined domain with a wealth on novel, challenging problems, as well as wide –ranging connections.

High-energy heavy-ion collision experiments worldwide are devoted to the investigation of strongly interacting matter under extreme conditions.

CBM experiment

The mission

Create highest baryon densities in nucleus-nucleus collisions. Explore the properties of super-dense nuclear matter. Search for in-medium modification of hadrons. Search for the transition from dense hadronic matter to quark-gluon matter, and for the critical endpoint in the phase diagram of strongly interacting matter.

The physics

Fundamental aspects of Quantum-Chromo-Dynamics and astrophysics: The equation-of-state of strongly interacting matter at high baryon densities, the restoration of chiral symmetry, the origin of hadron masses, the confinement of quarks in hadrons, the structure of neutron stars, the dynamics of core-collapse supernovae.

The challenge

Measure rare and penetrating probes such as dilepton pairs from light vector mesons and charmonium, open charm, multistrange hyperons, together with collective hadron flow and fluctuations in heavy-ion collisions at rates of up to 10 Million reactions per second.

The technique

Tracking and vertex reconstruction with Silicon pixel and strip detectors in a magnetic field, electron identification with Ring Imaging Cherenkov detectors and Transition Radiation Detectors, or, alternatively, muon identification with a muon detection system, time-of flight measurement with diamond strip detectors and Resistive Plate Chamber arrays. High speed signal processing and data acquisition.

 The goal of the experiment is to emsure multiplicities, phase distribution and flow of protons, pions, kaons, hyperons, hadronic resonances, light vector mesons, charmonium and open charm including their correlations and event-by enent fluctuations in heavy-ion collisions. The technical challenge of the CBM experiment is to identify both, hadrons and leptons, and to filter out rare probes at reaction rates of up to 10 MHz with carged particle multiplicities of up to 1000 per event. Measurements as these high rates cannot be performed with slow detectors , but rather require extremely fast and radiation hard detector components. Moreover, the experiment has to provide lepton identification, high-resolution secondary vertex determination and a high speed trigger and data acquisition system. The CBM detector system will have the capability to measure both electrons and muons.

The heart of the experiment will be a silicon tracking and vertex detection system installed in a large acceptance dipole magnet. The Silicon Tracking System (STM) consists of low mass silicon micro strip detectors possibly complemented by one or two hybrid-pixel detector layers providing unambiguous space point measurements. The STS allows for track reconstruction in a wide momentum range from about 100MeV up to more then 10GeV with a momentum resolution of about 1%.
 A key feature of the CBM experiment is online event selection which requires free streaming read-out electronics and fast algorithms running on computer farms based on future many-core arhitectures.
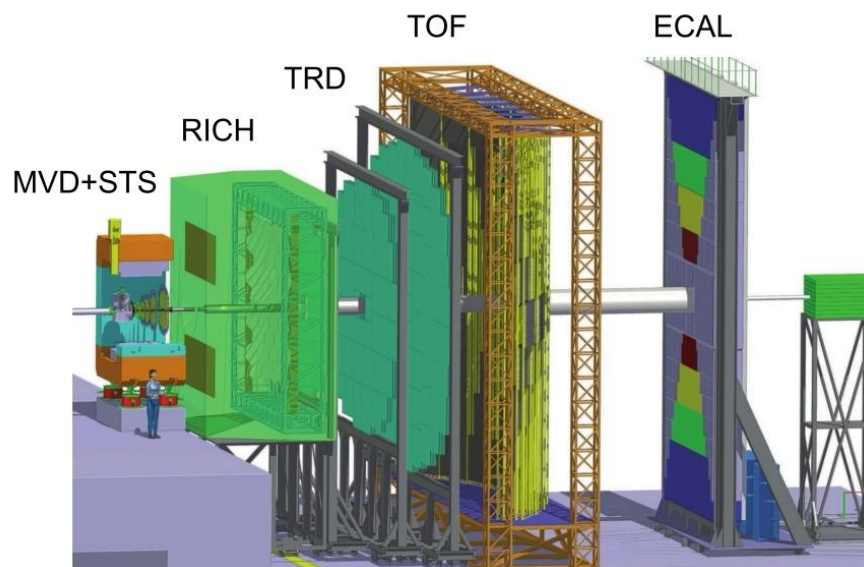

Fig. 1. The compressed Baryonic Matter (CBM) experiment.

VI.   References

I.   Plasma. An Analysis

http://en.wikipedia.org/wiki/Plasma_(physics)
N. A. Kapțov " Fenomene electrice în gaze și vid ", Editura Tehnică, 1955
Gheorghe Popa, Lucel Sîrghi " Bazele fizicii plasmei", Editura Universității " Alexandru Ioan   Cuza"
Iași, 2000
http ://thunder.msfc.nasa.gov
http ://fusedweb.llnl.gov

II.   Quantum Plasmas

1) Bengt ELIASSON and Padma K. SHUKLA, „ Nonlinear Aspects of Quantum Plasma Physics:Nanoplasmonics and Nanostructures in Dense Plasmas" , 16 April 2009
2) F. Haas, B. Eliasson, P. K. Shukla and G. Manfredi, „Phase-space structures in quantum-plasma wave turbulence"
3) S. V. Vladimirov and Yu. O. Tyshetskiy," On description of quantum plasma", January 24 2011

III.   Quarck-Gluon Plasma

1
L. Evans, *Eur. Phys. J. C* **34** (2004) 57, Proceedings of the ECFA-CERN Workshop on the Large Hadron Collider in the LEP tunnel, CERN 84-10 (1984).
2
Particle Data Group, *Phys. Lett. B* **667** (2008) 1,
J.R. Cudell, *et al.* (COMPETE Collaboration), *Phys. Rev. D* **65** (2002) 074024.
3
ALICE Collaboration, *J. Phys. Nucl. Part. Phys. G* **30** (2004) 1517–1763,
               J. Phys. Nucl. Part. Phys. G **32** (2006) 1295–2040.
4.
http://en.wikipedia.org/w/index.php?title=Quark%E2%80%93gluon_plasma#Thermodynamics
5.
Cheuk–Yin Wong, *Introduction to High Energy Heavy-Ion Collisions* (World Scientific, Singapore,1994) ISBN 9810202636.
6.
J. Lettessier and J. Rafelski, *Hadrons and Quark–Gluon Plasma,* Cambridge Monogaphs on Particle Physics, Nuclear Physics and Cosmology (Cambridge University Press, 2005) ISBN 0 521 01823 4.

7.

Relativistic heavy-ion physics- *G. Herrera Corral* [CERN, Geneva, Switzerland]

8.

"Energy loss of energetic partons in quark-gluon plasma: Possible extinction of high p_T jets in hadron-hadron collisions."--J.D. Bjorken- Fermi National Accelerator Laboratory

IV.   White Dwarfs

[1] Fowler, R. H., 1926, Mon. Not. R. Astr. Soc. 87, 114

[2] Chandrasekhar, S., Astrophys. J. 74, 81 (1931)

[6] Landau, L., Phys. Z. Sowjetunion 1, 285 (1932)

[8] Baade, W. and Zwicky, F., Phys. Rev. 45, 138 (1934)

[9] Baade, W. and Zwicky, F., Proc. Nat. Acad. Sci. 20, 254 (1934)

[1] L. Spruch, Reviews of Modern Physics **63**, 151 (1991).

[2] B. Schutz, *Gravity from the Ground Up: An Introductory Guide to Gravity and General Relativity* (Cambridge UniversityPress, 2003).

[3] E. Stoner, Philosophical Magazine **ix**, 944 (1930)

[4] S. Chandrasekhar, Astrophysical Journal **74**, 81 (1931)

[5] M. Rotondo, J. A. Rueda, R. Ruffini, and S.-S.Xue (2010)

[6] J. A. Rueda, M. Rotondo, R. Ruffini, and S.-S.Xue (2010)

[7] R. Feynman, N. Metropolis, and E. Teller, Physical Review **75**, 1561 (1949)

J.S. Kalirai, Astrophisics in White Dwarfs (2004)

Yan Zhu, A. Thomas, Fermi Approach to White Dwarfs (2011)

V.   Neutron Stars

http://en.wikipedia.org/wiki/Magnetar

http://www.princeton.edu/physics/

http://www.universe-galaxies-stars.com/archive_311.html

http://imagine.gsfc.nasa.gov/docs/science/know_l1/pulsars.html

Ryan Hamerly, 2005

B. Friman, C. Hohme, J. Knoll, S. Leupold, J. Randrup, R. Rapp, P. Senger, " The CBM Physics Book", February 4, 2011

http://www.gsi.de/forschung/fair_experiments/CBM/index_e.html

http://physis.ro

BACKGROUND

http://benabb.wordpress.com/2010/12/16/61839/

VII. Table of Colors

⬤	Alexandra Chilug, IonuțȘtefănescu, Dana Tudor, Lucian Tudor
⬤	Alin Ene, Marinel Negoi, Cristina Niță
⬤	Marinel Negoi
⬤	Andreea Dobre
⬤	Claudia Constantin
⬤	Nicoleta Dumitrescu
⬤	Simona Brajnicov, Alexandru Bălăceanu
⬤	Gheorghe Ungureanu
⬤	Sabina Simon, Bogdan Guȿter

ACKNOWLEDGEMENTS